The combination of the tubulin binding small molecule PTC596 and proteasome inhibitors suppresses the growth of myeloma cells

(微小管阻害薬 PTC596 とプロテアソーム阻害薬の

併用療法は骨髄腫細胞の増殖を抑制する)

千葉大学大学院医学薬学府

先端医学薬学専攻

(主任：横手　幸太郎教授)

長井　友莉恵

Abstract

The novel small molecule PTC596 inhibits microtubule polymerization and its clinical development has been initiated for some solid cancers. We herein investigated the preclinical efficacy of PTC596 alone and in combination with proteasome inhibitors in the treatment of multiple myeloma (MM). PTC596 inhibited the proliferation of MM cell lines as well as primary MM samples *in vitro*, and this was confirmed with MM cell lines *in vivo*. PTC596 synergized with bortezomib or carfilzomib to inhibit the growth of MM cells *in vitro*. The combination treatment of PTC596 with bortezomib exerted synergistic effects in a xenograft model of human MM cell lines in immunodeficient mice and exhibited acceptable tolerability. Mechanistically, treatment with PTC596 induced cell cycle arrest at G2/M phase followed by apoptotic cell death, associated with the inhibition of microtubule polymerization. RNA sequence analysis also revealed that PTC596 and the combination with bortezomib affected the cell cycle and apoptosis in MM cells. Importantly, endoplasmic reticulum stress induced by bortezomib was enhanced by PTC596, providing an underlying mechanism of action of the combination therapy. Our results indicate that PTC596 alone and in combination with proteasome inhibition are potential novel therapeutic options to improve outcomes in patients with MM.

Introduction

Over the past decade, the prognosis of multiple myeloma (MM) has improved dramatically due to the introduction of proteasome inhibitors and immunomodulatory drugs (IMiDs). Recently, monoclonal antibodies and new drugs targeting epigenetic regulation have also been added to the therapeutic options to improve patient outcome. However, MM remains an incurable disease associated with complex heterogeneity; therefore, innovative therapeutic strategies of multiple drug combination are needed to conquer it[1].

Proteasome inhibitors have dramatically changed the treatment strategies for multiple myeloma. Bortezomib, the first approved proteasome inhibitor, is widely used in combination therapies because of its effectiveness, tolerability, and combinability[2]. Bortezomib has various modes of action including induction of endoplasmic reticulum (ER) stress, upregulation of pro-apoptotic proteins, suppression of anti-apoptotic proteins, inhibition of NF-κB and its downstream anti-apoptotic genes, and dysregulation of the DNA repair pathway[3]; and therefore, it can be currently combined with a variety of drugs such as alkylating reagents, IMiDs[4], monoclonal anti-CD38 antibodies[5], and a histone deacetylase inhibitor[6]. Moreover, next-generation proteasome inhibitors carfilzomib and ixazomib are also available in the clinical practice. To increase therapeutic options for patients, clinical trials of the novel combination of bortezomib with a BCL-2 inhibitor, an XPO1 inhibitor, or a monoclonal anti-BCMA antibody are ongoing in MM (NCT02755597, NCT03110562, NCT04091126). In the preclinical stage, we have shown proteasome inhibitors-containing combination strategies using an IRE1α endoribonuclease domain inhibitor, a selective Akt inhibitor, and an EZH2/EZH1 dual inhibitor in the treatment of MM[7-9].

PTC596 was originally developed to target cancer stem cells with degradation of B-cell specific Moloney murine leukemia virus integration site 1 (BMI1), which is a component of PRC1 that maintains transcriptional repression of target genes via ubiquityl histone H2A

(uH2A)[10]. Recently, PTC596 has been recognized as a direct microtubule polymerization inhibitor in a preclinical study of pancreatic ductal adenocarcinoma[11]. PTC596 induces cytotoxicity with EC_{50} values of 30–200 nM in various tumor cell lines[12] and has preclinical effects on hematological malignancies such as acute myeloid leukemia and mantle cell leukemia[13,14]. Clinical trials of PTC596 are ongoing for glioma, leiomyosarcoma, and ovarian cancer. (NCT03605550, NCT03761095, NCT03206645). More recently, PTC596 has shown activity killing MM cells, alone and in combination with BH3 mimetics or epigenetic modulators[15]. In the current study, we focused on the preclinical activities and modes of action of PTC596 alone as well as in combination with proteasome inhibitors in MM.

Results

PTC596 induces cytotoxicity in MM cells

We first examined the cytotoxic effect of PTC596 alone on MM cells. PTC596 induced significant cytotoxicity in several MM cell lines, including bortezomib-resistant lines such as KMS-11/BTZ, and OMP-2/BTZ in MTS assays (Fig. 1A, B). PTC596 exhibited cytotoxicity against MM cells irrespective of *TP53* status (*TP53* wild-type: MM.1S, H929; *TP53* mutation: RPMI8226, U266, OPM-2, OPM-2/BTZ; *TP53* deletion: KMS-11, KMS-11/BTZ according to the IARC TP53 database[16]). The concentrations of PTC596 required to inhibit cell viability by 50% (cytotoxic concentration; CC_{50}) were quite low against all cell lines tested, ranging from 25 to 100 nM (Supplementary Table S1). We also evaluated the efficacy of PTC596 in MM cell lines co-cultured with bone marrow stromal cells (BMSCs) from patients with MM by BrdU proliferation assays. As reported[17], MM cells grew better when co-cultured with BMSCs than without BMSCs. PTC596 suppressed the proliferation of MM cells even in the presence of BMSCs (Fig. 1C).

In order to determine the efficacy of PTC596 in MM cells *in vivo*, we next generated subcutaneous xenograft models of MM.1S cells in NOG immunodeficient mice. PTC596 (12.5 mg/kg) or control vehicle was administered orally twice a week for 4 weeks. PTC596 significantly inhibited the growth of tumors implanted in mice ($p=0.022$ on day 18, $p=0.058$ on day 21; Fig. 1D) and prolonged the survival of mice as compared with the control ($p=0.0021$; Fig. 1E). PTC596 treatment was well tolerated with slight weight loss and mild diarrhea which immediately recovered after the end of treatment.

PTC596 inhibits microtubule polymerization and triggers cell cycle arrest in MM cells

PTC596 has recently been demonstrated to directly inhibit microtubule polymerization in pancreatic ductal adenocarcinoma[11]. Therefore, we investigated the effects of PTC596 on the

levels of soluble (unpolymerized) versus polymerized tubulin content in MM cells using protein lysates from vehicle- or PTC596-treated MM.1S cells with tubulin preservation buffer. Visualization of tubulin fractions by western blotting demonstrated that PTC596 treatment led to a near-complete loss of polymerized microtubules. In contrast, polymerized microtubules were increased in cells treated with paclitaxel, which stabilizes the microtubule polymer and protects it from disassembly[18] (Fig. 2A). These results supported the inhibitory function of PTC596 against microtubule polymerization.

Because microtubules play a critical role in the separation of chromosomes during mitosis, inhibition of microtubule polymerization results in mitotic arrest. Overnight treatment with PTC596 significantly increased MM cells in G2/M phase, suggesting that PTC596 induced G2/M cell cycle arrest (Fig. 2B). Annexin V staining also demonstrated that PTC596 treatment for 2 days induced massive apoptosis in MM cell lines in a dose-dependent manner (Fig. 2C). These results suggested that the cytotoxicity of PTC596 in MM cells is provoked by mitotic arrest and subsequent apoptosis.

Next, we evaluated the efficacy of PTC596 in primary MM cells derived from patients. We purified $CD138^+$ cells from the bone marrow (BM) of patients with MM and cultured them in the presence of PTC596 for 12–24 hours. Of note, PTC596 treatment significantly reduced the proportion of Annexin V-negative viable MM cells in culture (Fig. 2D).

PTC596 in combination with proteasome inhibitors exerts augmented cytotoxicity against MM cells

To enhance the therapeutic benefits of PTC596 in MM cells, we investigated the possible synergism between PTC596 and the proteasome inhibitor bortezomib, which is a first-line therapeutic agent in the treatment of MM. We treated MM.1S cells with increasing concentrations of PTC596 (0 to 90 nM) and bortezomib (0 to 3 nM) as a single agent or in

combination. After 2 days of culture, cells were analyzed using MTS assays. PTC596 and bortezomib did not show a synergistic cytotoxic effect on MM cells in suspension culture, showing a high combination index (CI), which defines synergism when the calculated number is less than 1 (Supplementary Fig. S1A, Supplementary Table S2B)[19]. In contrast, PTC596 and bortezomib exerted synergistic or additive cytotoxic effects with a CI less than or around 1 when MM cells were co-cultured with BMSCs derived from patients with MM, which mimics the BM microenvironment (Fig. 3A, Supplementary Fig. S2A, Supplementary Table S2A, S2C). PTC596 and carfilzomib, another proteasome inhibiter, also showed synergistic or additive cytotoxic effects on MM cells when those were co-cultured with BMSCs (Supplementary Fig. S3A, Supplementary Table S2D). We next performed Annexin V staining to evaluate apoptosis in the combination treatment. Apoptosis induced by PTC596 (50 nM) was significantly augmented by the combination with bortezomib (Fig. 3B). Enhanced apoptosis in the combination was confirmed by western blotting; the combination with PTC596 and bortezomib enhanced cleavage of caspases, which was accompanied by a reduction in MCL1 protein levels compared with each single treatment (Fig. 3C). Notably, PTC596 in combination with bortezomib also induced significant cytotoxicity in primary $CD138^+$ cells from the BM of patients with MM compared with bortezomib alone, as evidenced by reductions in Annexin V-negative viable cells (Fig. 3D).

To understand the effects of PTC596 on global transcriptional profiles in MM cells, we performed RNA-seq of MM.1S cells treated with PTC596 alone or in combination with bortezomib. Several gene sets related to cell cycle were negatively enriched in MM cells treated with PTC596 alone as well as PTC596 and bortezomib. In addition, apoptosis-related gene sets were positively enriched in MM cells treated with PTC596 and bortezomib (Fig. 3E and Supplementary Table S3-S6).

PTC596 and bortezomib demonstrate synergistic effects in a xenograft model of human myeloma cells

In order to evaluate the efficacy of the combination of PTC596 with bortezomib *in vivo*, we used subcutaneous xenograft models of MM.1S cells, as shown in Fig. 1D and E. PTC596 (6.25 mg/kg) was administered orally to mice in combination with subcutaneous injections of bortezomib (0.5 mg/kg) twice a week for 5 weeks. The combination therapy of PTC596 and bortezomib significantly reduced tumor growth compared with the control (day 29, $p<0.001$), PTC596 alone (day 29, $p<0.001$), and bortezomib alone (day 32, $p=0.010$) (Fig. 4A). Survival of host mice treated with the combination was significantly prolonged compared with the control ($p<0.001$), PTC596 alone ($p<0.001$), and bortezomib alone ($p=0.007$) (Fig. 4B). Of note, 1 out of 12 mice treated with combination therapy achieved a complete response with no residual tumor. Mice which received the combination therapy did not show significant body weight loss except one that needed a washout period of the drugs until recovery (Fig. 4C). Hematological toxicity was examined in another cohort, in which the mice were treated with or without oral PTC596 in combination with or without subcutaneous bortezomib for 2 weeks. White blood cell counts and hemoglobin levels in the peripheral blood of mice did not change significantly during treatment with PTC596 or even the combination (Fig. 4D, E). These results demonstrated that PTC596 in combination with bortezomib is effective and tolerable *in vivo*, holding promise of clinical applications.

PTC596 functions independently of BMI1 in MM cells

PTC596 was initially identified as an agent decreasing the levels of BMI1 protein[12,13], which plays an oncogenic role in the maintenance of proliferative capacity of cells through repression of the *INK4a*/*ARF* pathway[20,21]. BMI1 becomes hyperphosphorylated and dissociates from chromatin during mitosis[22], suggesting that PTC596 induces reductions in BMI1 protein levels

as an indirect consequence of induction of mitotic arrest. The functional role of BMI1 in the activity of PTC596 has been tested in *Kras*/*p53* mutant pancreatic tumors, in which deletion of *Bmi1* did not affect the ability of PTC596 to inhibit cell proliferation[11]. Of interest, bortezomib was reported to repress the transcription of *BMI1* in the side population of mantle cell lymphoma cells[23] and reduce the levels of mono-ubiquitination of histone H2A at Lysine 119 (uH2A)[24]. However, its impact on BMI1 in MM cells has not yet been elucidated. We examined *BMI1* mRNA levels by qPCR and the protein levels of BMI1 and uH2A by western blotting after bortezomib treatment in MM cells (Fig. 5A, B). Bortezomib significantly repressed the expression of *BMI1* and reduced the protein levels of BMI1 and uH2A. The combination treatment of PTC596 with bortezomib had additive effects on the levels of BMI1 and uH2A (Fig. 5C).

In order to evaluate the functional role of BMI1 in the activity of PTC596 alone and in combination with bortezomib, we determined BMI1 target genes in MM cells using MM.1S cells overexpressing mouse Bmi1 (mBmi1) by ChIP-seq as reported previously [25]. We defined 3517 genes with enrichment of Bmi1 signals over the input signals by 2.5-fold from the promoter regions (transcription start sites ± 2.0 kb) as direct targets of BMI1 (Fig. 5D). We then checked the correlation between expression levels and fold enrichment values (IP/input) of Bmi1 (Fig. 5E). The expression levels of these genes were inversely correlated with the fold enrichment values of Bmi1 (Fig. 5E). We then checked the expression levels of BMI1 targets after PTC596 treatment alone or in combination with bortezomib. Unexpectedly, PTC596 alone or in combination with bortezomib did not significantly de-repress the expression of BMI1 target genes in spite of significant reductions in BMI1 protein levels (Fig. 5F). These results supported the notion that PTC596 functions independently of BMI1.

PTC596 enhanced endoplasmic reticulum stress induced by bortezomib

In order to elucidate the target pathways of PTC596 and the mechanism underlying the synergistic effect with bortezomib, we analyzed RNA-seq data using g:profiler[26]. Genes up-regulated upon treatment with PTC596 or bortezomib as single agents largely overlapped. Of interest, endoplasmic reticulum (ER)-related gene ontology terms were significantly enriched in 5299 overlapping genes (Fig. 6A, Supplementary Table S7). RT-PCR analyses revealed the upregulation of representative ER stress-related genes, such as *DDIT3* (also known as CHOP or GADD153), *HSPA5* (also known as BiP or GRP78), and *ATF4*, by bortezomib treatment and to a lesser extent by PTC596 treatment. Of note, the expression of ER stress-related genes induced by bortezomib[27] was significantly enhanced by the combination treatment (Fig. 6B). Among ER stress-related genes, *DDIT3* encodes a transcriptional factor CHOP which is related to fatal ER stress[27]. We confirmed that the protein levels of CHOP and BiP were elevated by the combination treatment by western blotting (Fig. 6C). Importantly, knockdown of *ATF4* and *DDIT3* by shRNA lead to the suppression of the cytotoxicity of the combination treatment, indicating that the ER stress pathway at least partially contributes to the synergy of PTC596 with bortezomib (Supplementary Fig. S4)

To look at the upregulation of ER stress pathways by the combination treatment *in vivo,* we performed western blotting and RT-PCR using tumors harvested from NOG mice treated with or without oral PTC596 in combination with or without subcutaneous bortezomib for 2 weeks. The protein levels of CHOP were enhanced by the combination treatment (N=2, Supplementary Fig. S5A). We also confirmed that the mRNA expression of *DDIT3* and *ATF4* in the tumors was elevated by the combination treatment (Supplementary Fig. S5B). These data indicated that augmented ER stress is one of the mechanisms of action in this combination.

Discussion

In this study, we demonstrated the activities of a novel tubulin binding agent PTC596 alone and in combination with proteasome inhibitors in MM both *in vitro* and *in vivo*. As reported recently in pancreatic ductal adenocarcinoma[11], we confirmed that PTC596 inhibits tubulin polymerization in MM cells. PTC596-induced G2/M cell cycle arrest in MM cells may be attributed to the inhibitory effect of PTC596 against microtubule polymerization[28]. PTC596 significantly induced cytotoxicity against MM cell lines, primary MM cells, as well as MM cells in a xenograft model *in vivo*. Moreover, PTC596 induced significant cytotoxicity in MM cell lines regardless of bortezomib sensitivity or the status of *TP53* gene mutations and deletions, which are closely related to shorter survival, poor response, and resistance to drugs in MM [29] . These results indicated the sufficient preclinical efficacy of PTC596 in the treatment of MM, consistent with the recent report[15].

As therapeutic strategies for MM, combination treatments including proteasome inhibitors or IMiDs are crucial to control this heterogeneous disease[30]. We found that combination treatment of PTC596 and proteasome inhibitors exerted additive or synergistic cytotoxicity in MM. Our *in vivo* data using a xenograft model demonstrated that this combination is promising, with definitive synergy and acceptable tolerability. Of note, fatal ER stress was identified as a possible mechanism of action in the combination of PTC596 with bortezomib. ER stress plays an important role in the development of MM and its pathway is a therapeutic target for proteasome inhibitors[31]. The ER stress pathway is also the target for the synergistic effects of combination treatments using various agents with bortezomib in MM[7,8,32,33]. We demonstrated that the transcription factor CHOP, a surrogate maker of fatal ER stress, was elevated in the combination of PTC596 with bortezomib compared with each single treatment. Although the mechanism by which PTC596 enhanced bortezomib-inducing ER stress is still unclear, a microtubule degrader N-deacetyl-N-(chromone-2-carbonyl)-

thiocolchicine has been reported to induce ER stress-mediated cytotoxicity in hepatocellular carcinoma cells[34]. Podophyllotoxin acetate, which inhibits microtubule polymerization, also activates the ER stress pathway in non-small cell lung cancer cells[35]. These reports indicated that the microtubule disruption as well as inhibition of microtubule polymerization induce activation of the ER stress pathway.

MCL1 can be another target of PTC596 as a single agent as well as in combination with bortezomib. MCL1, an anti-apoptotic protein, is essential for MM cell survival and related to relapse and poor prognosis[36]. In the present study, PTC596 decreased MCL1 levels in MM cells, as reported previously in acute myeloid leukemia and mantle cell lymphoma[13,14]. Bortezomib treatment compromises the anti-apoptotic function of MCL1 by promoting its proteolytic cleavage[37,38]. Additive effects of PTC596 and bortezomib on the reduction of full length MCL1 protein may account for enhanced apoptosis with the combination therapy in MM cells.

As reported previously[13,14], PTC596 reduced the levels of BMI1 and ubiquitination of H2A in MM cell lines. PTC596 reportedly induces the reduction in BMI1 via its phosphorylation at 2 N-terminal sites[12-14,39]; however, BMI1 becomes hyperphosphorylated and dissociates from chromatin during mitosis[11], suggesting that PTC596 induces reductions in BMI1 protein levels as an indirect consequence of the induction of mitotic arrest. BMI1 plays an essential role in MM cell progression, survival, and drug resistance[40,41]. We confirmed that MM cells depend on BMI1 for their growth (Supplementary Fig. S6). However, unexpectedly, BMI1 target genes in MM cells were not significantly de-repressed by PTC596 treatment, suggesting that PTC596 functions independently of BMI1. Supporting our findings, a recent report has demonstrated that BMI1 is not required for the anti-MM activity of PTC596[15]. Nevertheless, bortezomib significantly downregulated BMI1 in MM cells as reported in mantle cell lymphoma cells[23], and PTC596 enhanced the bortezomib-induced reductions in BMI1

protein levels in MM cells. Because depletion of *BMI1* was reported to enhance the sensitivity of MM cells to bortezomib[42], the cooperative effects of PTC596 and bortezomib on BMI1 protein levels might be another mechanism of the synergistic action of this combination.

In conclusion, our findings demonstrate that microtubule polymerization inhibition alone and in combination with proteasome inhibition are potential novel therapeutic options in MM. This study provides a preclinical framework for the clinical evaluation of this promising therapeutic approach to improve outcomes in patients with MM.

Author's Contribution

Y. Nagai designed research, performed experiments, analyzed data, and actively wrote the manuscript; N. Mimura and A. Iwama (co-corresponding authors) conceived and designed research, analyzed data, and actively wrote the manuscript; O. Rizq, Y. Isshiki, M. Oshima, M. Rizk, A. Saraya, S. Koide, Y. Nakajima-Takagi, and M. Miyota performed experiments; N. Oshima-Hasegawa, T. Muto, S. Tsukamoto, S. Mitsukawa, Y. Takeda, C. Ohwada, M. Takeuchi, T. Iseki, C. Nakaseko, and E. Sakaida analyzed data and provided clinical samples; T. Chiba and K. Yokote analyzed data; and W. Lennox, J. Sheedy, and M. Weetall contributed the vital new reagent.

Acknowledgments

The authors thank D. Shinoda, M. Takahashi, and A. Koga for their technical assistance. The super-computing resource was provided by the Human Genome Center, the Institute of Medical Science, the University of Tokyo. This work was supported in part by Grants-in-Aid for Scientific Research in Japan (#19K08807, #19H05653), Scientific Research on Innovative Areas "Replication of Non-Genomic Codes" (#19H05746) from MEXT, Japan; and grants from the Uehara Memorial Foundation, the Yasuda Medical Foundation, the Mochida Memorial Foundation, the Kanae Foundation for the promotion of Medical Science, and the Chiba University SEEDS Fund (Chiba University Open Recruitment for International Exchange Program).

Conflict of interest disclosure

W.L., J.S., and M.W. are employed by PTC Therapeutic and have received salary compensation for time, effort, and hold or held financial interests in the company. The remaining authors declare no competing financial interests.

Materials and methods

Reagents

PTC596 was developed and provided by PTC Therapeutics, South Plainfield, NJ, USA. It was diluted in DMSO to make 20 mM or 1 mM stocks for *in vitro* experiments. For *in vivo* experiments, it was diluted in 0.5% (w/v) hydroxypropyl methylcellulose solution with 0.1% (w/v) Tween 80 to make a 12.5 mg/mL stock. Bortezomib and carfilzomib for *in vitro* experiments was obtained from Selleck Chemicals and diluted in DMSO to make a 100 μM stock. Bortezomib for *in vivo* experiments was purchased from Janssen Pharmaceutical KK and was diluted in normal saline to make a 1 mg/mL stock. Paclitaxel was purchased from Sigma-Aldrich and was diluted in DMSO to make a 10 mM stock.

Human MM cell lines and primary cells

Human MM cell lines MM.1S, NCI-H929 (H929), U266, and RPMI8226 were obtained from the American Type Culture Collection. Human KMS11 and bortezomib-resistant KMS11/BTZ[43] cells were obtained from the Japanese Collection of Research Bioresources Cell Bank. Human OPM-2 plasma cell leukemia cell line was kindly provided by Dr. Edward Thompson (University of Texas Medical Branch, Galveston, TX). Bortezomib-resistant OPM-2/BTZ[43] was obtained from Kyowa Kirin Co., Ltd. MM cells were cultured in RPMI 1640 containing 10% fetal bovine serum (FBS), 2 μM L-glutamine, 100 U/mL penicillin, and 100 μg/mL streptomycin (Thermo Fisher).

Human samples from patients

Primary MM cells and BMSCs were collected from the bone marrow of patients with newly diagnosed or relapsed refractory MM at Chiba University Hospital. All patients provided written informed consent in accordance with the declaration of Helsinki and patient anonymity

was ensured. This study was approved by the Institutional Review Committee at Chiba University (Approval #964 and #1025). Plasma cells and BMSCs were purified as previously described[9] and were cultured in Dulbecco's modified Eagle's medium supplemented with 10% FBS, 2 μM L-glutamine, 100 U/mL penicillin, and 100 μg/mL streptomycin (Thermo Fisher).

Co-culture experiments

BMSCs were plated and cultured in a 96 well plate for 24 hours and then MM cells were added and treated with PTC596 in combination with bortezomib or carfilzomib for the indicated times. Then the samples were analyzed by assays of cytotoxicity.

Assays of cytotoxicity

To evaluate the cytotoxicity of PTC596 alone and in combination with proteasome inhibitors, MTS and BrdU ELISA assays were performed using human MM cell lines. In MTS assay, CellTiter 96 AQueous One Solution (Promega) was added to the cells in the last 4 hours of the incubation period and absorbance was read on a plate reader as described previously[9]. For BrdU ELISA assay, BrdU cell proliferation ELISA kits (colorimetric; Abcam and Roche) were used in accordance with the manufacturer's instructions. The absorbance of BMSCs alone was subtracted from each value when MM cells were co-cultured with BMSCs.

Murine xenograft models of human MM

Male NOD/Shi-scid, IL-2RγKOJic (NOG) mice were purchased from CLEA Japan Inc. Animal studies of xenograft models were conducted according to Chiba University guidelines for the use of laboratory animals and approved by the Review Board for Animal Experiments of Chiba University (approval #1-92).

NOG mice were injected subcutaneously on the right side of the back with 4×10^6 MM.1S cells in 100 μL RPMI 1640. After the tumor grew to a measurable size, treatment was initiated. For the PTC596 single treatment described in Fig. 1D and E, the mice were treated with oral PTC596 (12.5 mg/kg) or control vehicle twice a week for 4 weeks. For the combination treatment of PTC596 with bortezomib, the mice were treated with oral PTC596 (6.25 mg/kg) and subcutaneous saline twice a week; subcutaneous bortezomib (0.5 mg/kg) in the left side of the back and orally administered vehicle twice a week; or oral PTC596 (6.25 mg/kg) twice a week and subcutaneous bortezomib (0.5 mg/kg) twice a week. Control mice received orally administered vehicle and subcutaneous saline. For the evaluation of tumor volume and survival analysis described in Fig.4A, 4B and 4C, the mice were treated for 5 weeks. Tumor volume was calculated from caliper measurements every 3–4 days until the day of the first death in each group. The mice were sacrificed when the tumors reached 2,000 cm^3 or an ulcer occurred. Survival was evaluated from the first day of treatment to death. Hematological toxicity described in Fig. 4D, 4E and the ER-stress induction described in Supplementary Fig. S5 were examined in another cohort, in which the mice were treated with or without oral PTC596 (6.25 mg/kg) twice a week in combination with or without subcutaneous bortezomib (0.5 mg/kg) twice a week for 2 weeks.

Western blotting

MM cells were lysed and sonicated prior to SDS-PAGE as described previously[9]. Tumors harvested from NOG mice were homogenized using a TissueRuptor (Qiagen) and lysed in RIPA (50 mM Tris, pH 8.0, 150 mM NaCl,1mM EDTA, pH 8.0,1% TritonX-100, 0.1% sodium deoxycholate and 0.1% SDS) buffers with protease inhibitor cocktail (Roche). Then Lysates were sonicated using a Bioruptor (COSMO BIO CO.) The supernatants were separated after

centrifugation and mixed with SDS-sample buffer (25mM Tris, pH6.8, 1% SDS, 5% glycerol, 0.05% bromophenol blue and 1%-mercaptoethanol).

Immunoblotting was performed using the following antibodies: anti-BMI1(Bethyl), anti-uH2A, anti-H2A, anti-caspase-3, anti-caspase-8, anti-caspase-9, anti-PARP, anti-CHOP, anti-BiP, and anti-GAPDH (Cell Signaling), anti-MCL1 (Santa Cruz) and anti-α-tubulin (Calbiochem). Whole blots are available in the Supplementary Information file.

Immunoblotting analysis of soluble versus polymerized tubulin

MM.1S cells were treated with PTC596 or paclitaxel for 4 hours. As reported previously[44], after washing by PBS, the cells were permeabilized with 200 μL of pre-warmed buffer [80 mM PIPES-KOH, 2 mM $MgCl_2$, 0.5 mM EGTA, 0.2% Triton X-100, 10% glycerol, 1×Protease inhibitor, pH 6.9] and incubated for 5 min at 30°C. The supernatants containing the soluble fraction of microtubules were separated after centrifugation and mixed with 4× Laemmli gel sample buffer. To collect the insoluble (polymerized) tubulin fraction, 1× Laemmli gel sample buffer (250 μL) was added to the pellet. These samples were boiled for 3 min. Microtubules were detected by western blotting with anti-α-tubulin antibodies.

Analysis of cell cycle and apoptosis by flow cytometry

An FITC BrdU Flow kit (BD Pharmigen) was used for cell cycle analysis in MM cells, and an FITC Annexin V Apoptosis Detection Kit I (BD Pharmingen) was used for the detection of apoptotic MM cells, in accordance with the manufacturer's instructions. Flow cytometry was performed using a BD FACS Canto II (BD Biosciences), and the obtained data were analyzed using FlowJo software (Tree Star).

RNA sequencing

Total RNA was isolated from ~1.0×10^6 MM.1S or OPM-2 cells using an RNeasy Mini Kit (QIAGEN). RNA concentration and integrity were verified using an Agilent 2100 Bioanalyzer (Santa Clara, CA, USA). Amplification, preparation of the libraries, and RNA sequencing (RNA-seq) were performed as described previously[45,46].

TopHat (version 1.3.2; with default parameters) was used to align with the human reference genome (hg19 from University of California, Santa Cruz Genome Browser; http://genome.ucsc.edu/). Then, gene expression values were calculated as reads per kilobase of exon unit per million mapped reads (RPKM) using cufflinks (version 2.0.2).

Quantitative RT-PCR

Total RNA was purified using an RNeasy Mini Kit or RNeasy plus micro kit (QIAGEN). cDNA was made using the ThermoScript RT-PCR system (Invitrogen) or a PrimeScript™ RT reagent Kit (Perfect Real Time) (Takara) with an oligo-dT primer. Quantitative RT-PCR was performed on a StepOnePlus Real-Time PCR System (Thermo Fisher Scientific) by using TB Green™ Premix Ex Taq™ GC (Perfect Real Time) (Takara). All data were examined in triplicate and presented as relative expression levels normalized to *GAPDH* or *ACTB* (β-actin) expression. The sequences of forward and reverse primers are shown in Supplementary Table S8.

Vector and virus production

A retroviral vector and virus were made using the same method as described previously[47]. *Mouse Bmi1 (mBmi1)* cDNA tagged with a 3×Flag in the retroviral vector pGCDNsam was used for the overexpression of mBmi1 to perform mBmi1 chromatin immunoprecipitation sequencing (ChIP-seq). For *BMI1* knockdown experiments, lentiviral vectors expressing short hairpin RNA (shRNA) that target human *BMI1* (sh-*BMI1*) and *luciferase* (sh-*Luc*) were

produced as described previously[48]. Knockdown experiments of *DDIT3* and *ATF4* were performed using lentiviral vectors: pLV[shRNA]-EGFP:T2A:Puro-U6>hATF4[sh-*ATF4#1*], pLV[shRNA]-EGFP:T2A:Puro-U6>hATF4[sh-*ATF4#2*], pLV[shRNA]-EGFP:T2A:Puro-U6>hDDIT3[sh-*DDIT3#1*], pLV[shRNA]-EGFP:T2A:Puro-U6>hDDIT3[sh-*DDIT3#2*] and pLV[shRNA]-EGFP/Puro-U6>Scramble_shRNA[sh-Scramble], constructed by VectorBuilder. Short hairpin sequences used in this study are sh-*DDIT3#1*: CTGCACCAAGCATGAACAATT, sh-*DDIT3#2*: TGAACGGCTCAAGCAGGAAAT, sh-*ATF4#1*: CATGATCCCTCAGTGCATAAA, sh-*ATF4#2*: TGAACGGCTCAAGCAGGAAAT. Recombinant retroviruses and lentiviruses were produced using established methods[49].

Chromatin immunoprecipitation sequencing

mBmi1 ChIP-seq was performed in mBmi1-overexpressing MM.1S cells as described previously[50]. Immunoprecipitation was performed using an anti-FLAG antibody (Sigma). Sheep anti-mouse IgG Dynabeads were used to capture the antibody.

Bowtie2 (version 2.2.6; default parameters) was used to map the reads to the reference genome (UCSC/mm10). Peaks were called using MACS2 v2.1.1 with a q-value of <0.1 for mBMI1. ChIP peaks that overlapped with those of a corresponding input (distance between centers <10 kb) were removed. Reads per million mapped reads (RPM) values of the sequenced reads were calculated for every 1,000 bp bin, with a shifting size of 100 bp using Bedtools. To visualize with Integrative GenomicsViewer (Broad Institute), the RPM values of the immunoprecipitated samples were normalized by subtracting the RPM values of the input samples in each bin and converted to a Bigwig file using the Wigtobigwig tool. In order to evaluate the mark of each gene, the RPM values of the region from 2 kb upstream to 2 kb downstream of the TSS of immunoprecipitated samples were divided by the RPM of the corresponding input.

Statistical analysis

The statistical significance of differences was measured using an unpaired two-tailed Student's *t*-test or Welch's *t*-test when the variance was judged as significantly different.

For multiple comparisons of combination treatments, one-way ANOVA test and Tukey's test were performed. P values less than 0.05 were considered significant, using Graph Pad Prism, version 8. Survival analysis by Kaplan–Meier curves and log-rank analysis were performed using Graph Pad Prism, version 8. The combination index (CI) of PTC596 with bortezomib was analyzed by isobologram analysis using Compu-Syn software (ComboSyn, Inc.)[19]. CI values of less than 1.0, equal to 1.0, and greater than 1.0 indicate synergistic, additive, and antagonistic effects, respectively.

Deposition of data

RNA sequence data were deposited in the DNA Data Bank of Japan (DDBJ) (accession number: DRA009600).

References

1 Mimura, N., Hideshima, T. & Anderson, K. C. Novel therapeutic strategies for multiple myeloma. *Experimental hematology* **43**, 732-741, doi:10.1016/j.exphem.2015.04.010 (2015).

2 Merin, N. M. & Kelly, K. R. Clinical use of proteasome inhibitors in the treatment of multiple myeloma. *Pharmaceuticals (Basel)* **8**, 1-20, doi:10.3390/ph8010001 (2014).

3 Mujtaba, T. & Dou, Q. P. Advances in the understanding of mechanisms and therapeutic use of bortezomib. *Discov Med* **12**, 471-480 (2011).

4 Ito, S. Proteasome Inhibitors for the Treatment of Multiple Myeloma. *Cancers* **12**, doi:10.3390/cancers12020265 (2020).

5 Palumbo, A. *et al.* Daratumumab, Bortezomib, and Dexamethasone for Multiple Myeloma. *New England Journal of Medicine* **375**, 754-766, doi:10.1056/NEJMoa1606038 (2016).

6 San-Miguel, J. F. *et al.* Panobinostat plus bortezomib and dexamethasone versus placebo plus bortezomib and dexamethasone in patients with relapsed or relapsed and refractory multiple myeloma: a multicentre, randomised, double-blind phase 3 trial. *The Lancet. Oncology* **15**, 1195-1206, doi:10.1016/s1470-2045(14)70440-1 (2014).

7 Mimura, N. *et al.* Blockade of XBP1 splicing by inhibition of IRE1alpha is a promising therapeutic option in multiple myeloma. *Blood* **119**, 5772-5781, doi:10.1182/blood-2011-07-366633 (2012).

8 Mimura, N. *et al.* Selective and potent Akt inhibition triggers anti-myeloma activities and enhances fatal endoplasmic reticulum stress induced by proteasome inhibition. *Cancer Res* **74**, 4458-4469, doi:10.1158/0008-5472.can-13-3652 (2014).

9 Rizq, O. *et al.* Dual Inhibition of EZH2 and EZH1 Sensitizes PRC2-Dependent Tumors to Proteasome Inhibition. *Clinical cancer research : an official journal of the American*

Association for Cancer Research **23**, 4817-4830, doi:10.1158/1078-0432.ccr-16-2735 (2017).

10 Cao, L. *et al.* BMI1 as a novel target for drug discovery in cancer. *Journal of cellular biochemistry* **112**, 2729-2741, doi:10.1002/jcb.23234 (2011).

11 Eberle-Singh, J. A. *et al.* Effective delivery of a microtubule polymerization inhibitor synergizes with standard regimens in models of pancreatic ductal adenocarcinoma. *Clinical Cancer Research*, clincanres.3281.2018, doi:10.1158/1078-0432.ccr-18-3281 (2019).

12 Kim, M. J. *et al.* Abstract 5517: PTC596-induced Bmi1 hyper-phosphorylation via Cdk1/2 activation resulting in tumor stem cell depletion. *Cancer Research* **74**, 5517-5517, doi:10.1158/1538-7445.am2014-5517 (2014).

13 Nishida, Y. *et al.* The novel BMI-1 inhibitor PTC596 downregulates MCL-1 and induces p53-independent mitochondrial apoptosis in acute myeloid leukemia progenitor cells. *Blood Cancer J* **7**, e527, doi:10.1038/bcj.2017.8 (2017).

14 Maeda, A. *et al.* Targeting of BMI-1 expression by the novel small molecule PTC596 in mantle cell lymphoma. *Oncotarget* **9**, 28547-28560, doi:10.18632/oncotarget.25558 (2018).

15 Bolomsky, A. *et al.* The anti-mitotic agents PTC-028 and PTC596 display potent activity in pre-clinical models of multiple myeloma but challenge the role of BMI-1 as an essential tumour gene. *British journal of haematology*, doi:10.1111/bjh.16595 (2020).

16 Olivier, M. *et al.* The IARC TP53 database: new online mutation analysis and recommendations to users. *Human mutation* **19**, 607-614, doi:10.1002/humu.10081 (2002).

17 Hideshima, T., Mitsiades, C., Tonon, G., Richardson, P. G. & Anderson, K. C. Understanding multiple myeloma pathogenesis in the bone marrow to identify new

therapeutic targets. *Nature Reviews Cancer* **7**, 585, doi:10.1038/nrc2189 (2007).

18 Rowinsky, E. K. & Donehower, R. C. Paclitaxel (taxol). *The New England journal of medicine* **332**, 1004-1014, doi:10.1056/nejm199504133321507 (1995).

19 Chou, T. C. & Talalay, P. Quantitative analysis of dose-effect relationships: the combined effects of multiple drugs or enzyme inhibitors. *Advances in enzyme regulation* **22**, 27-55 (1984).

20 Jacobs, J. J., Kieboom, K., Marino, S., DePinho, R. A. & van Lohuizen, M. The oncogene and Polycomb-group gene bmi-1 regulates cell proliferation and senescence through the ink4a locus. *Nature* **397**, 164-168, doi:10.1038/16476 (1999).

21 Siddique, H. R. & Saleem, M. Role of BMI1, a stem cell factor, in cancer recurrence and chemoresistance: preclinical and clinical evidences. *Stem cells (Dayton, Ohio)* **30**, 372-378, doi:10.1002/stem.1035 (2012).

22 Voncken, J. W. *et al.* Chromatin-association of the Polycomb group protein BMI1 is cell cycle-regulated and correlates with its phosphorylation status. *Journal of cell science* **112 (Pt 24)**, 4627-4639 (1999).

23 Teshima, K. *et al.* Dysregulation of BMI1 and microRNA-16 collaborate to enhance an anti-apoptotic potential in the side population of refractory mantle cell lymphoma. *Oncogene* **33**, 2191-2203, doi:10.1038/onc.2013.177 (2014).

24 Xu, Q., Farah, M., Webster, J. M. & Wojcikiewicz, R. J. Bortezomib rapidly suppresses ubiquitin thiolesterification to ubiquitin-conjugating enzymes and inhibits ubiquitination of histones and type I inositol 1,4,5-trisphosphate receptor. *Mol Cancer Ther* **3**, 1263-1269 (2004).

25 Nitta, E. *et al.* Bmi1 counteracts hematopoietic stem cell aging by repressing target genes and enforcing the stem cell gene signature. *Biochemical and biophysical research communications*, doi:10.1016/j.bbrc.2019.10.153 (2019).

26 Raudvere, U. *et al.* g:Profiler: a web server for functional enrichment analysis and conversions of gene lists (2019 update). *Nucleic acids research* **47**, W191-w198, doi:10.1093/nar/gkz369 (2019).

27 Obeng, E. A. *et al.* Proteasome inhibitors induce a terminal unfolded protein response in multiple myeloma cells. *Blood* **107**, 4907-4916, doi:10.1182/blood-2005-08-3531 (2006).

28 Mukhtar, E., Adhami, V. M. & Mukhtar, H. Targeting microtubules by natural agents for cancer therapy. *Molecular cancer therapeutics* **13**, 275-284, doi:10.1158/1535-7163.MCT-13-0791 (2014).

29 Avet-Loiseau, H. *et al.* Genetic abnormalities and survival in multiple myeloma: the experience of the Intergroupe Francophone du Myelome. *Blood* **109**, 3489-3495, doi:10.1182/blood-2006-08-040410 (2007).

30 Paul, B., Lipe, B., Ocio, E. M. & Usmani, S. Z. Induction Therapy for Newly Diagnosed Multiple Myeloma. *American Society of Clinical Oncology educational book. American Society of Clinical Oncology. Annual Meeting* **39**, e176-e186, doi:10.1200/edbk_238527 (2019).

31 Nikesitch, N., Lee, J. M., Ling, S. & Roberts, T. L. Endoplasmic reticulum stress in the development of multiple myeloma and drug resistance. *Clin Transl Immunology* **7**, e1007-e1007, doi:10.1002/cti2.1007 (2018).

32 Hideshima, T. *et al.* Discovery of selective small-molecule HDAC6 inhibitor for overcoming proteasome inhibitor resistance in multiple myeloma. *Proceedings of the National Academy of Sciences of the United States of America* **113**, 13162-13167, doi:10.1073/pnas.1608067113 (2016).

33 Wallington-Beddoe, C. T. *et al.* Sphingosine kinase 2 inhibition synergises with bortezomib to target myeloma by enhancing endoplasmic reticulum stress. *Oncotarget*

8, 43602-43616, doi:10.18632/oncotarget.17115 (2017).

34 Ho, C.-T. *et al.* A Novel Microtubule-Disrupting Agent Induces Endoplasmic Reticular Stress-Mediated Cell Death in Human Hepatocellular Carcinoma Cells. *PloS one* **10**, e0136340-e0136340, doi:10.1371/journal.pone.0136340 (2015).

35 Choi, J. Y. *et al.* Podophyllotoxin acetate triggers anticancer effects against non-small cell lung cancer cells by promoting cell death via cell cycle arrest, ER stress and autophagy. *International journal of oncology* **47**, 1257-1265, doi:10.3892/ijo.2015.3123 (2015).

36 Wuilleme-Toumi, S. *et al.* Mcl-1 is overexpressed in multiple myeloma and associated with relapse and shorter survival. *Leukemia* **19**, 1248-1252, doi:10.1038/sj.leu.2403784 (2005).

37 Gomez-Bougie, P. *et al.* Noxa up-regulation and Mcl-1 cleavage are associated to apoptosis induction by bortezomib in multiple myeloma. *Cancer Res* **67**, 5418-5424, doi:10.1158/0008-5472.can-06-4322 (2007).

38 Podar, K. *et al.* A pivotal role for Mcl-1 in Bortezomib-induced apoptosis. *Oncogene* **27**, 721-731, doi:10.1038/sj.onc.1210679 (2008).

39 Dey, A. *et al.* Evaluating the Mechanism and Therapeutic Potential of PTC-028, a Novel Inhibitor of BMI-1 Function in Ovarian Cancer. *Mol Cancer Ther* **17**, 39-49, doi:10.1158/1535-7163.mct-17-0574 (2018).

40 Jagani, Z. *et al.* The Polycomb group protein Bmi-1 is essential for the growth of multiple myeloma cells. *Cancer Res* **70**, 5528-5538, doi:10.1158/0008-5472.CAN-09-4229 (2010).

41 Bolomsky, A., Schlangen, K., Schreiner, W., Zojer, N. & Ludwig, H. Targeting of BMI-1 with PTC-209 shows potent anti-myeloma activity and impairs the tumour microenvironment. *J Hematol Oncol* **9**, 17, doi:10.1186/s13045-016-0247-4 (2016).

42 Wu, S. Q., Xu, Z. Z., Niu, W. Y., Huang, H. B. & Zhan, R. ShRNA-mediated Bmi-1 silencing sensitizes multiple myeloma cells to bortezomib. *Int J Mol Med* **34**, 616-623, doi:10.3892/ijmm.2014.1798 (2014).

43 Ri, M. *et al.* Bortezomib-resistant myeloma cell lines: a role for mutated PSMB5 in preventing the accumulation of unfolded proteins and fatal ER stress. *Leukemia* **24**, 1506-1512, doi:10.1038/leu.2010.137 (2010).

44 Punganuru, S. R. *et al.* Conception, synthesis, and characterization of a rofecoxib-combretastatin hybrid drug with potent cyclooxygenase-2 (COX-2) inhibiting and microtubule disrupting activities in colon cancer cell culture and xenograft models. *Oncotarget* **9**, 26109-26129, doi:10.18632/oncotarget.25450 (2018).

45 Mochizuki-Kashio, M. *et al.* Ezh2 loss in hematopoietic stem cells predisposes mice to develop heterogeneous malignancies in an Ezh1-dependent manner. *Blood* **126**, 1172-1183, doi:10.1182/blood-2015-03-634428 (2015).

46 Rizk, M. *et al.* Akt inhibition synergizes with polycomb repressive complex 2 inhibition in the treatment of multiple myeloma. *Cancer science* **110**, 3695-3707, doi:10.1111/cas.14207 (2019).

47 Konuma, T. *et al.* Forced expression of the histone demethylase Fbxl10 maintains self-renewing hematopoietic stem cells. *Experimental hematology* **39**, 697-709.e695, doi:10.1016/j.exphem.2011.03.008 (2011).

48 Chiba, T. *et al.* Bmi1 promotes hepatic stem cell expansion and tumorigenicity in both Ink4a/Arf-dependent and -independent manners in mice. *Hepatology (Baltimore, Md.)* **52**, 1111-1123, doi:10.1002/hep.23793 (2010).

49 Iwama, A. *et al.* Enhanced self-renewal of hematopoietic stem cells mediated by the polycomb gene product Bmi-1. *Immunity* **21**, 843-851, doi:10.1016/j.immuni.2004.11.004 (2004).

50 Isshiki, Y. *et al.* KDM2B in polycomb repressive complex 1.1 functions as a tumor suppressor in the initiation of T-cell leukemogenesis. *Blood advances* **3**, 2537-2549, doi:10.1182/bloodadvances.2018028522 (2019).

Figure legends

Figure 1. PTC596 inhibits the growth of MM cells both *in vitro* and *in vivo*.

(A, B) MTS assays of (A) MM.1S, H929, RPMI8226, U266, and (B) KMS-11, KMS-11/BTZ, OPM-2, OPM-2/BTZ treated with the indicated doses of PTC596 for 72 hours. The y-axis presents percent viability relative to the untreated control. Data are shown as means ± SD of triplicate or quadruplicate samples. (C) Cell proliferation assays evaluated by BrdU incorporation of MM.1S and OPM2 cells co-cultured with or without BMSCs isolated from patients with MM upon treatment with the indicated doses of PTC596 for 48 hours. BrdU was added to the culture 2 hours before the analysis. Y-axis is presented as proliferation rate relative to an untreated control. Data are shown as mean ± SD of triplicate samples. $*P < 0.05$; $**P < 0.01$; $***P < 0.001$; ns, not significant by a one-way ANOVA. (D, E) *In vivo* analysis of the cytotoxicity of PTC596 using a murine xenograft model of human myeloma MM.1S cells. NOG mice were injected subcutaneously on the right side of the back with 4×10^6 MM.1S cells. After the tumor grew to a measurable size, treatment was initiated. Mice were treated with oral PTC596 (12.5 mg/kg) (n=7) or control vehicle (n=6) twice a week for 4 weeks. (D) Tumor volumes were monitored twice a week. Data represent mean ± SEM. $*P < 0.05$ using Student's *t*-test. (E) Kaplan–Meier survival of mice. The mice were sacrificed when the tumors reached 2,000 cm^3 or an ulcer occurred. Survival was evaluated from the first day of treatment to death. The statistical significance of differences between PTC596-treated and vehicle-treated groups was determined using a log-rank test. $**P < 0.01$.

Figure 2. PTC596 induces cell cycle arrest and apoptosis associated with the inhibition of microtubule polymerization.

(A) Western blotting analysis of soluble and polymerized microtubules in MM cells detected using an anti-α-tubulin antibody. MM.1S were incubated in the presence or absence of PTC596

or paclitaxel for 4 hours. After treatment, cell lysates were fractionated by centrifugation to separate free tubulin (soluble tubulin) from microtubules (polymerized tubulin). The graphs show the density volumes of α-tubulin normalized to that of the soluble fraction in the control. (B) Cell cycle analysis of MM.1S and H929 treated with the indicated doses of PTC596 for 24 hours, exposed to BrdU for 2 hours, followed by flow cytometric analyses. Data represent mean ± SD of triplicate experiments. *$P < 0.05$; ***$P < 0.001$; ns, not significant using one-way ANOVA. (C) Annexin V staining of MM.1S and OPM-2 treated with the indicated doses of PTC596 for 48 hours. Apoptotic cells were detected as Annexin V-positive cells by flow cytometry. The representative flow cytometric profiles are shown in the left panels, and the results of duplicate experiments are shown in the right graphs. Data represent mean ± SD. **$P < 0.01$; ***$P < 0.001$; ns, not significant using one-way ANOVA. (D) The cytotoxicity of the indicated doses of PTC596 against primary MM cells analyzed by Annexin V staining using flow cytometry. Primary MM cells were treated for 12–24 hours. Data represent mean ± SD of duplicate experiments. *$P < 0.05$; **$P < 0.01$; ***$P < 0.001$ using Student's *t*-test or one-way ANOVA.

Figure 3. PTC596 enhances bortezomib-induced apoptosis

(A) BrdU proliferation assay of MM.1S co-cultured with BMSCs derived from patients with MM upon treatment with the indicated doses of PTC596 and bortezomib for 48 hours. Results of triplicate experiments and combination index values are shown in the left and right graphs, respectively. (B) Annexin V staining of OPM-2 treated with the indicated doses of PTC596 for 48 hours and bortezomib for 24 hours. Apoptotic cells were detected as Annexin V-positive cells by flow cytometry, and the results of duplicate experiments are shown. Data represent mean ± SD. *$P < 0.05$; **$P < 0.01$; ns, not significant using one-way ANOVA. (C) Western blotting analysis of the indicated proteins in MM.1S and OPM-2. MM.1S and OPM-2 were

treated with PTC596 (100 nM) and/or bortezomib (2 nM for MM.1S and 5 nM for OPM-2) for 48 hours. GAPDH served as a loading control. (D) The cytotoxicity of the combination treatment of PTC596 and bortezomib against primary MM cells. Viable cells were defined as those negative for Annexin V and PI by flow cytometric analyses. Primary MM cells were treated with the indicated doses of PTC596 and/or bortezomib for 12 or 24 hours. Data represent mean ± SD. *$P < 0.05$; **$P < 0.01$; n.s., not significant using Student's *t*-test or one-way ANOVA. (E) Gene set enrichment analysis plots showing the enrichment of cell cycle or apoptosis gene sets in MM.1S treated with PTC596 alone (left panels) and the combination (right panels) compared with non-treated control cells. MM.1S cells were treated with PTC596 (100 nM) alone or in combination with bortezomib (2 nM) for 24 hours. Total RNA was extracted and RNA-seq was performed. Normalized enrichment scores (NES), nominal p values (NOM), and false discovery rates (FDR) are indicated.

Figure 4. PTC596 and bortezomib exert synergistic anti-MM activity in a xenograft MM model.

NOG mice were injected subcutaneously on the right side of the back with 4×10^6 MM.1S cells. After the tumor grew to a measurable size, treatment was initiated. Mice were treated for 5 weeks with oral PTC596 (6.25 mg/kg) twice a week, subcutaneous bortezomib (0.5 mg/kg) in the left side of the back twice a week, or the combination. Control mice received orally administered vehicle and subcutaneous saline for 5 weeks. (A) Tumor volume was monitored twice a week in PTC596-treated group (n=11), bortezomib-treated group (n=11), combination group (n=12), and vehicle-treated group (n=12). Data represent mean ± SEM. *$P < 0.05$; ***$P < 0.001$ using one-way ANOVA and Student's *t*-test. (B) Kaplan–Meier survival of mice. The mice were sacrificed when the tumors reached 2,000 cm^3 or an ulcer occurred. Survival was evaluated from the first day of treatment to death. Statistical significance was determined using

the log-rank test. $^{**}P < 0.01$; $^{***}P < 0.001$. (C) Body weight of the mice. Data represent mean ± SD. (D) White blood cell counts and (E) Hemoglobin (Hb) of the mice examined on the indicated day of treatment. Data represent mean ± SD.

Figure 5. PTC596 does not directly target BMI1.

(A) Quantitative RT-PCR analysis of *BMI1* in MM.1S treated with the indicated dose of bortezomib for 24 hours. *GAPDH* was used to normalize the amount of input RNA. Data are shown as the mean ± SD (n=3). $^{**}P < 0.01$; n.s., not significant using one-way ANOVA. (B) Western blotting analysis of BMI1 and uH2A in MM.1S and OPM-2 upon treatment with the indicated doses of bortezomib for 48 hours. GAPDH and H2A served as loading controls. (C) Western blotting analysis of BMI1 and uH2A in MM.1S and OPM-2 upon treatment with PTC596 (100 nM) and bortezomib (2 nM for MM.1S and 5 nM for OPM-2) alone or in combination for 48 hours. GAPDH and H2A served as loading controls. (D) Bmi1 targets defined by ChIP-seq data of Bmi1. Graph showing the number of genes in each range of fold enrichment values (IP/input) of Bmi1. Genes with 2.5-fold enrichment of Bmi1 signals over the input signals in the promoter regions (transcription start sites ± 2.0 kb) were defined as direct targets of BMI1 (red bars). (E) Expression levels of all RefSeq genes and BMI1 target genes detected by RNA-seq (RPKM). Bmi1 target genes with fold enrichment greater than 2.5, 3.0, and 4.0 are depicted separately. $^{**}P < 0.01$; n.s., not significant using Welch's *t*-test. (F) Box-and-whisker plots showing the expression changes of 351 BMI1 target genes in MM.1S cells treated with PTC596 alone (left panel) and PTC596 in combination with bortezomib (right panel) compared with control cells. Boxes represent 25 to 75 percentile ranges. Vertical lines represent 10 to 90 percentile ranges. Horizontal bars represent median. ns, not significant using Student's *t*-test.

Figure 6. Endoplasmic reticulum stress is augmented by the combination of PTC596 and bortezomib.

(A) Venn diagram of 9110 genes upregulated upon PTC596 treatment and 8662 genes upregulated upon bortezomib treatment, compared with the control, in RNA-seq analysis. Gene ontology terms related to endoplasmic reticulum were significantly enriched in 5299 overlapping genes. (B) Quantitative RT-PCR analysis of *BMI1* in MM.1S treated with or without PTC596 (100 nM) for 48 hours in the presence or absence of bortezomib (2.5 nM) for 24 hours. *ACTB* was used to normalize the amount of input RNA. Data are shown as mean ± SD (n=3). $^{**}P < 0.01$; $^{***}P < 0.001$; ns, not significant using one-way ANOVA. (C) Western blotting analysis of the indicated proteins in MM.1S. MM.1S were treated with or without PTC596 (100 nM) for 48 hours in the presence or absence of bortezomib (2.5 nM) for 24 hours. GAPDH served as a loading control. The right graphs show the density volume normalized by GAPDH.

Figure 1.

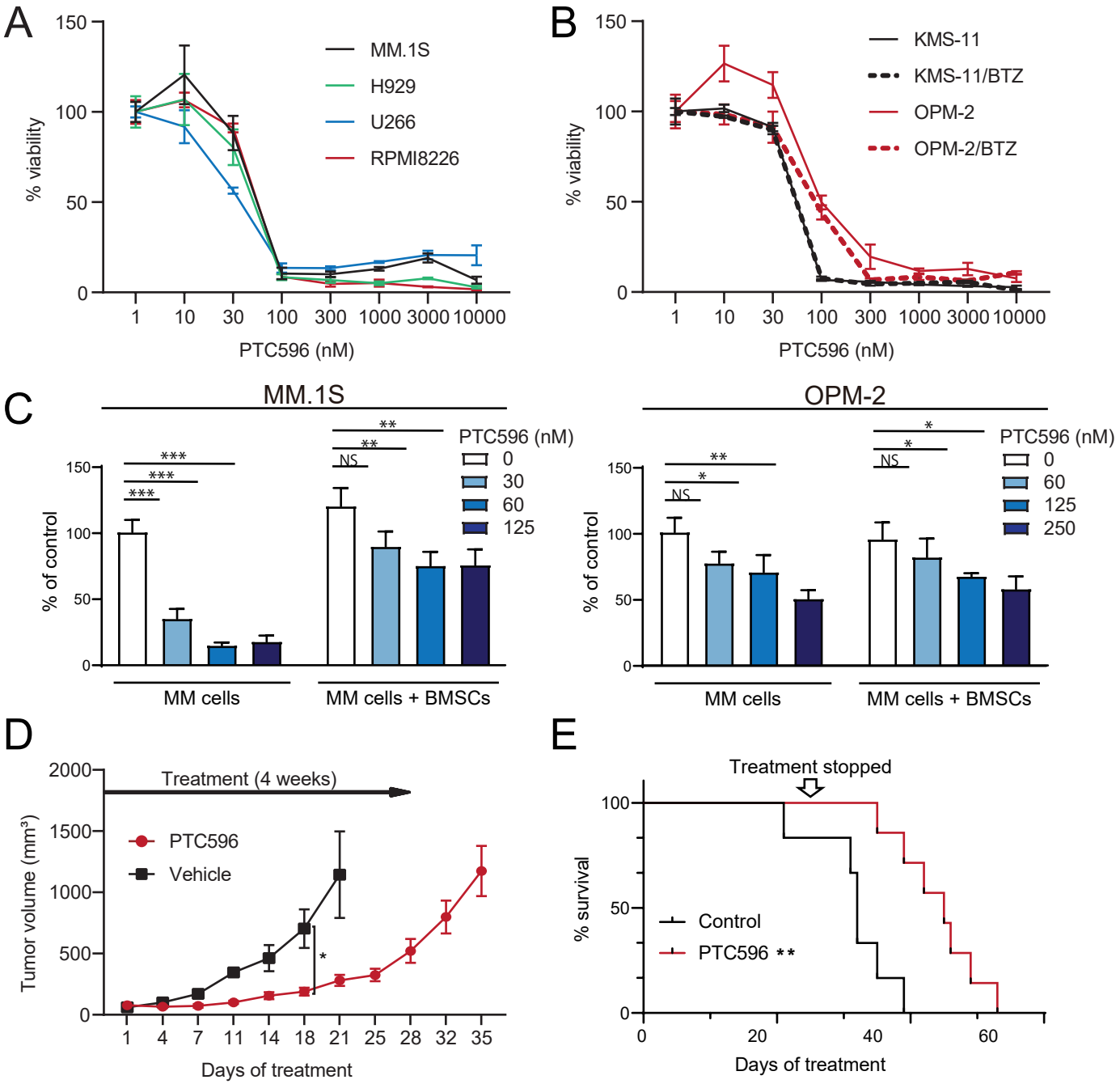
A
% viability
MM.1S
H929
U266
RPMI8226
PTC596 (nM)
B
% viability
KMS-11
KMS-11/BTZ
OPM-2
OPM-2/BTZ
PTC596 (nM)
C
MM.1S
OPM-2
% of control
PTC596 (nM)
MM cells
MM cells + BMSCs
NS
D
Treatment (4 weeks)
PTC596
Vehicle
Tumor volume (mm³)
Days of treatment
E
Treatment stopped
% survival
Control
PTC596 **
Days of treatment

Figure 2.

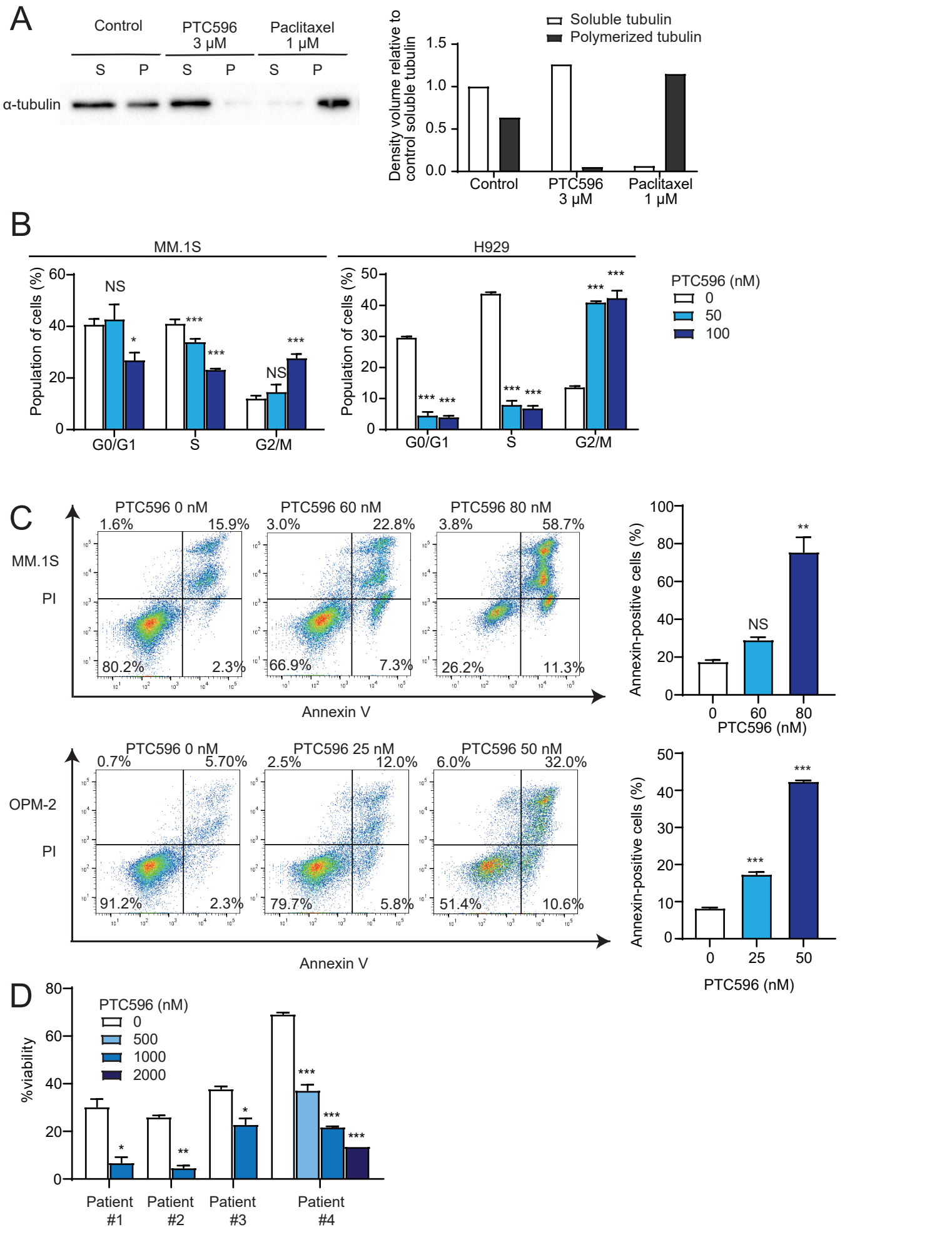
A
Control
PTC596 3 μM
Paclitaxel 1 μM
S
P
S
P
S
P
α-tubulin
Soluble tubulin
Polymerized tubulin
Density volume relative to control soluble tubulin
1.5
1.0
0.5
0.0
Control
PTC596 3 μM
Paclitaxel 1 μM
B
MM.1S
H929
Population of cells (%)
60
40
20
0
NS
*
***
***
***
NS
G0/G1
S
G2/M
50
40
30
20
10
0
***
***
***
***
***
***
G0/G1
S
G2/M
PTC596 (nM)
0
50
100
C
MM.1S
PI
PTC596 0 nM
1.6%
15.9%
80.2%
2.3%
PTC596 60 nM
3.0%
22.8%
66.9%
7.3%
PTC596 80 nM
3.8%
58.7%
26.2%
11.3%
Annexin V
Annexin-positive cells (%)
100
80
60
40
20
0
**
NS
0
60
80
PTC596 (nM)
OPM-2
PI
PTC596 0 nM
0.7%
5.70%
91.2%
2.3%
PTC596 25 nM
2.5%
12.0%
79.7%
5.8%
PTC596 50 nM
6.0%
32.0%
51.4%
10.6%
Annexin V
Annexin-positive cells (%)
50
40
30
20
10
0
***
***
0
25
50
PTC596 (nM)
D
%viability
80
60
40
20
0
PTC596 (nM)
0
500
1000
2000
*
**
*
***
***
***
Patient #1
Patient #2
Patient #3
Patient #4

Figure 3.

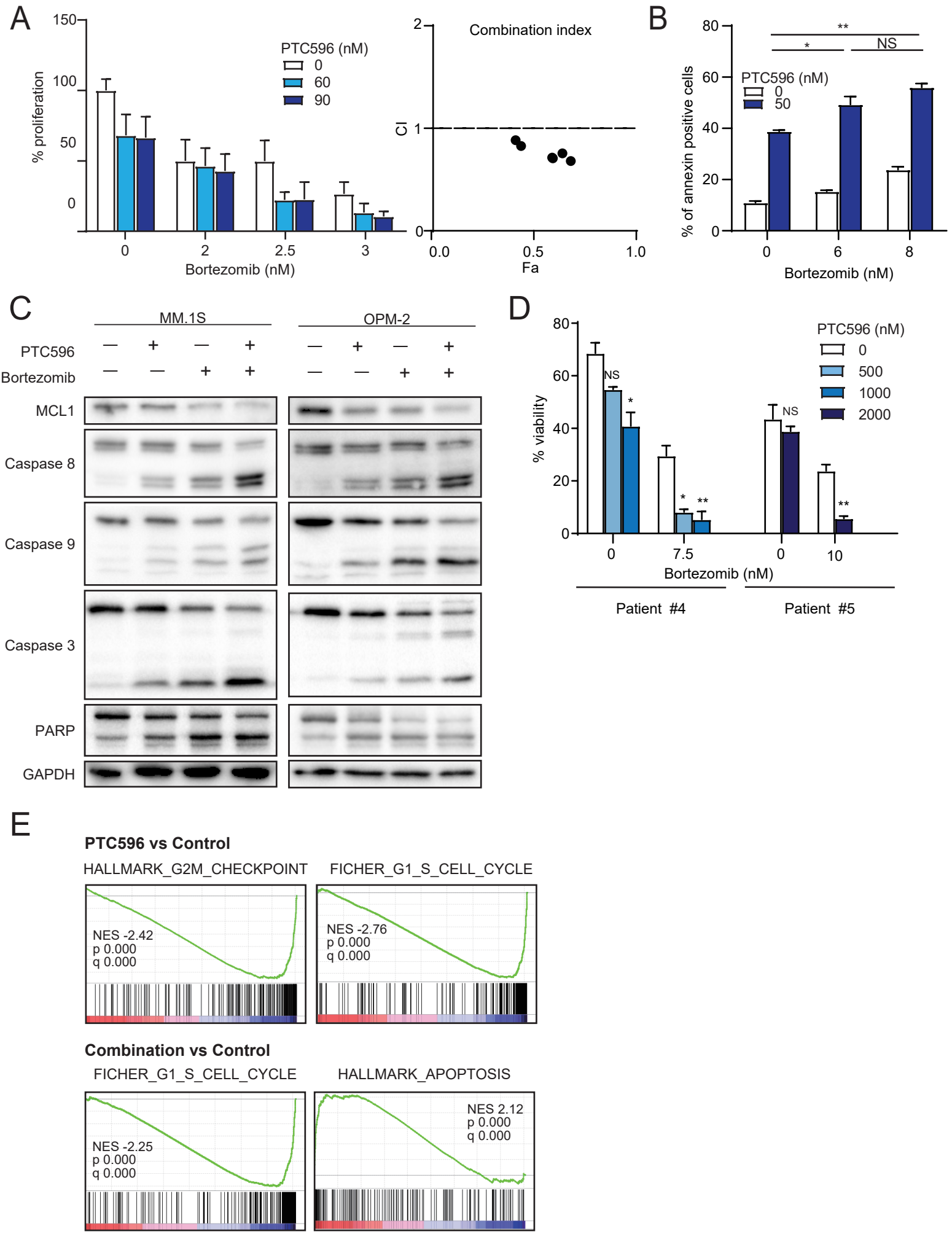
A
% proliferation
PTC596 (nM)
0
60
90
Bortezomib (nM)
Combination index
CI
Fa
B
% of annexin positive cells
PTC596 (nM)
0
50
NS
Bortezomib (nM)
C
MM.1S
OPM-2
PTC596
Bortezomib
MCL1
Caspase 8
Caspase 9
Caspase 3
PARP
GAPDH
D
% viability
PTC596 (nM)
0
500
1000
2000
NS
Bortezomib (nM)
Patient #4
Patient #5
E
PTC596 vs Control
HALLMARK_G2M_CHECKPOINT
NES -2.42
p 0.000
q 0.000
FICHER_G1_S_CELL_CYCLE
NES -2.76
p 0.000
q 0.000
Combination vs Control
FICHER_G1_S_CELL_CYCLE
NES -2.25
p 0.000
q 0.000
HALLMARK_APOPTOSIS
NES 2.12
p 0.000
q 0.000

Figure 4.

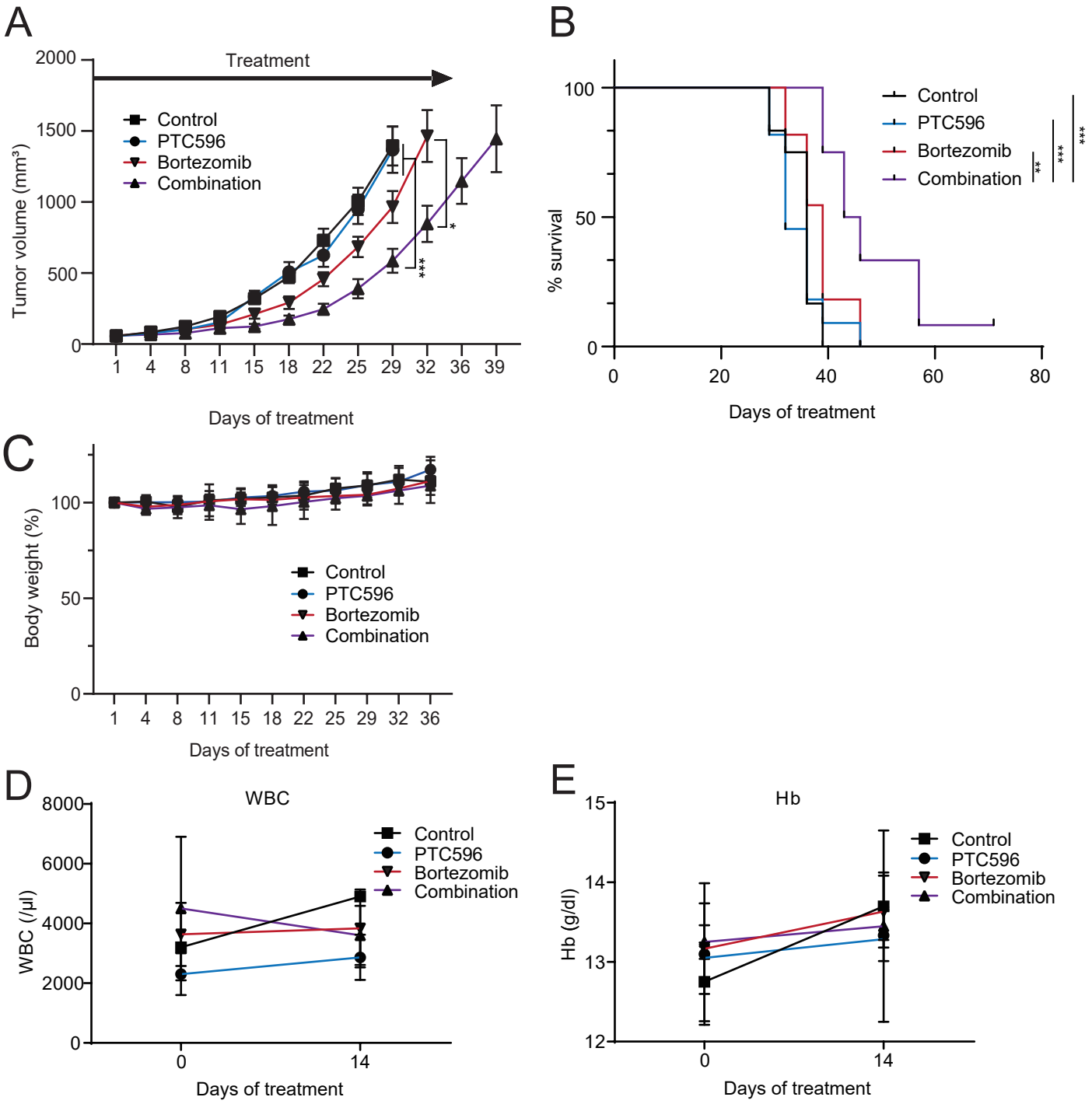
A
Treatment
Control
PTC596
Bortezomib
Combination
Tumor volume (mm³)
2000
1500
1000
500
0
1 4 8 11 15 18 22 25 29 32 36 39
Days of treatment
***
*
B
Control
PTC596
Bortezomib
Combination
% survival
100
50
0
0 20 40 60 80
Days of treatment
**
***
***
C
Body weight (%)
100
50
0
Control
PTC596
Bortezomib
Combination
1 4 8 11 15 18 22 25 29 32 36
Days of treatment
D
WBC
WBC (/μl)
8000
6000
4000
2000
0
Control
PTC596
Bortezomib
Combination
0 14
Days of treatment
E
Hb
Hb (g/dl)
15
14
13
12
Control
PTC596
Bortezomib
Combination
0 14
Days of treatment

Figure 5.

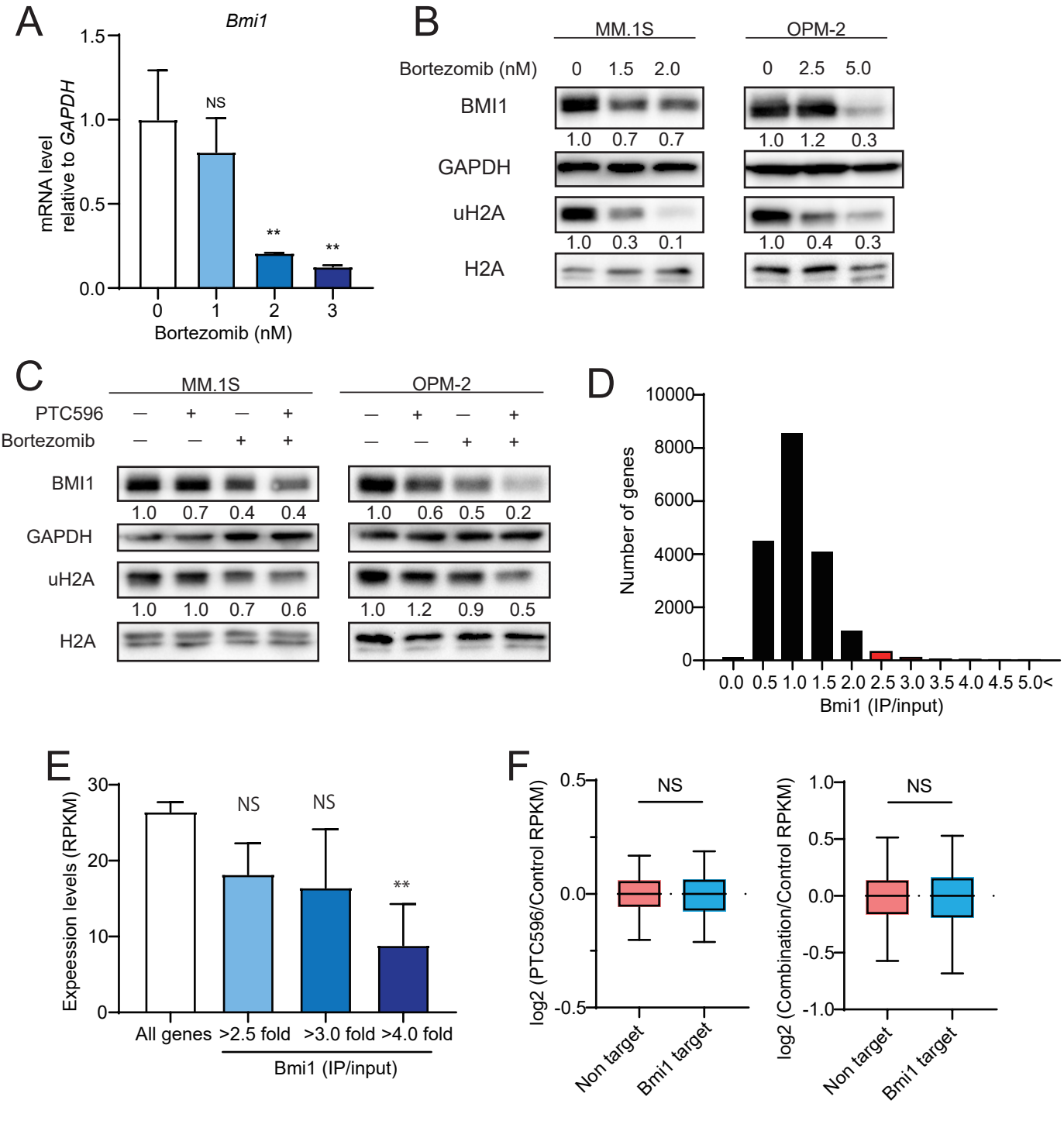
A
Bmi1
mRNA level relative to GAPDH
1.5
1.0
0.5
0.0
NS
**
**
0
1
2
3
Bortezomib (nM)
B
MM.1S
OPM-2
Bortezomib (nM)
0
1.5
2.0
0
2.5
5.0
BMI1
1.0 0.7 0.7
1.0 1.2 0.3
GAPDH
uH2A
1.0 0.3 0.1
1.0 0.4 0.3
H2A
C
MM.1S
OPM-2
PTC596
Bortezomib
BMI1
1.0 0.7 0.4 0.4
1.0 0.6 0.5 0.2
GAPDH
uH2A
1.0 1.0 0.7 0.6
1.0 1.2 0.9 0.5
H2A
D
Number of genes
10000
8000
6000
4000
2000
0
0.0 0.5 1.0 1.5 2.0 2.5 3.0 3.5 4.0 4.5 5.0<
Bmi1 (IP/input)
E
Expeession levels (RPKM)
30
20
10
0
NS
NS
**
All genes
>2.5 fold
>3.0 fold
>4.0 fold
Bmi1 (IP/input)
F
log2 (PTC596/Control RPKM)
0.5
0.0
-0.5
NS
Non target
Bmi1 target
log2 (Combination/Control RPKM)
1.0
0.5
0.0
-0.5
-1.0
NS
Non target
Bmi1 target

Figure 6.

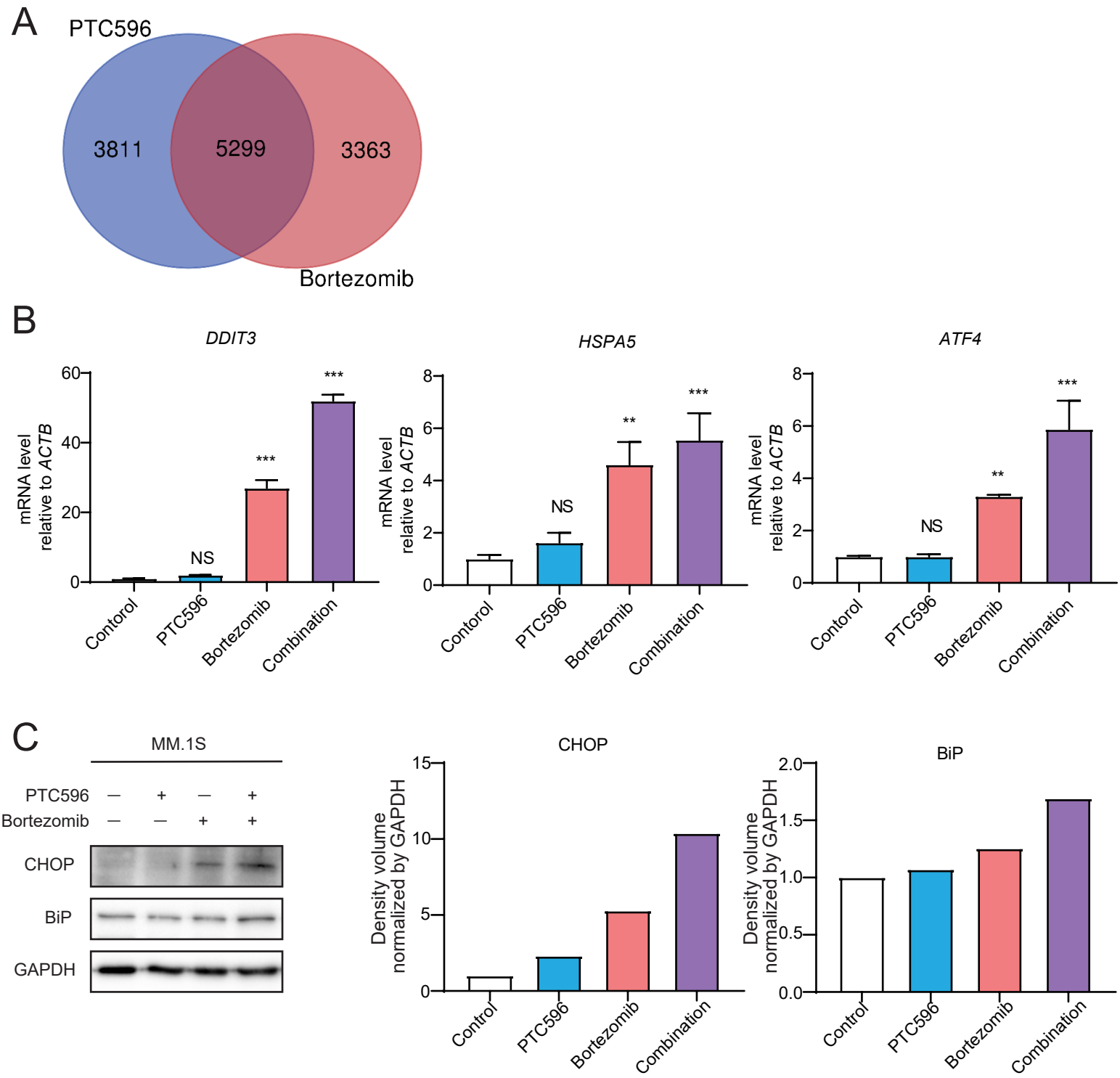
A
PTC596
3811
5299
3363
Bortezomib
B
DDIT3
HSPA5
ATF4
mRNA level relative to ACTB
NS
Contorol
PTC596
Bortezomib
Combination
C
MM.1S
PTC596
Bortezomib
CHOP
BiP
GAPDH
Density volume normalized by GAPDH
Control

The combination of the tubulin binding small molecule PTC596 and proteasome inhibitors suppresses the growth of myeloma cells

Yurie Nagai

Supporting Information:

Supplementary Tables S1-S8

Supplementary Figures and legends S1-S6

Whole blots for cropped images

Supplementary Table S1.

CC_{50} values of cell lines calculated from the results of MTS assays described in Figure 1A, B.

	MM.1S	H929	U266	RPMI 8226	KMS-11	KMS-11 /BTZ	OPM-2	OPM-2 /BTZ
CC50 [nM]	45.58	44.03	24.19	50.75	49.46	48.33	97.74	74.21

Supplementary Table S2.

The combination effect of two agents was analyzed by isobologram analysis with Compu-Syn software (ComboSyn, Inc).

(A) CI values of MM.1S cells treated with the combination of PTC596 and bortezomib in a BrdU proliferation assay (Figure 3A).

(B) CI values of MM.1S cells treated with the combination of PTC596 and bortezomib in an MTS assay (Figure S1).

(C) CI values of OPM-2 cells treated with the combination of PTC596 and bortezomib in a BrdU proliferation assay (Figure S2).

(D) CI values of MM.1S cells treated with the combination of PTC596 and carfilzomib in a BrdU proliferation assay (Figure S3).

Supplementary Table S2A

PTC596 [nM]	Bortezomib [nM]	Fa	CI
60.0	2.0	0.4031	0.88409
60.0	2.5	0.5842	0.70830
60.0	3.0	0.6315	0.75578
90.0	2.0	0.4296	0.82729
90.0	2.5	0.5813	0.71339
90.0	3.0	0.6719	0.68030

Supplementary Table S2B

PTC596 [nM]	Bortezomib [nM]	Fa	CI
20.0	4.0	0.1804	1.28328
20.0	5.0	0.5075	1.12710
40.0	4.0	0.2120	1.50260
40.0	5.0	0.6441	1.12023
60.0	4.0	0.4290	1.30784
60.0	5.0	0.5819	1.29851
80.0	4.0	0.5004	1.34579
80.0	5.0	0.6145	1.36450

Supplementary Table S2C

PTC596 [nM]	Bortezomib [nM]	Fa	CI
60.0	4.0	0.6469	1.01406
60.0	5.0	0.8250	1.06931
125.0	4.0	0.8491	0.88074
125.0	5.0	0.8385	1.09679
250.0	4.0	0.7795	1.07512
250.0	5.0	0.8790	1.09907

Supplementary Table S2D

PTC596 [nM]	Carfilzomib [nM]	Fa	CI
15	3	0.4271	1.20322
15	4	0.7983	0.86478
15	5	0.9473	0.77541
30	3	0.8492	0.63050
30	4	0.9374	0.65286
30	5	0.9562	0.75073

Supplementary Table S3.

Significantly upregulated gene sets in MM.1S cells treated with PTC596.

Gene set enrichment analysis using our RNA-seq data identified gene sets, which were significantly enriched in MM.1S cells treated with PTC596 versus control. (FDR w-value <0.01).

c2.all.v7.0

NAME	SIZE	NES	NOM p-val	FDR q-val
MACAEVA_PBMC_RESPONSE_TO_IR	96	2.42	0.000	0.000
KERLEY_RESPONSE_TO_CISPLATIN_UP	43	2.33	0.000	0.001

Supplementary Table S4.

Significantly downregulated gene sets in MM.1S cells treated with PTC596.

Gene set enrichment analysis using our RNA-seq data identified gene sets, which were significantly downregulated in MM.1S cells treated with PTC596 versus control. (FDR w-value <0.01).

Hallmark

NAME	SIZE	NES	NOM p-val	FDR q-val
HALLMARK_E2F_TARGETS	196	-3.03	0.000	0.000
HALLMARK_G2M_CHECKPOINT	189	-2.42	0.000	0.000
HALLMARK_MYC_TARGETS_V1	197	-2.34	0.000	0.000
HALLMARK_ESTROGEN_RESPONSE_LATE	164	-2.00	0.000	0.002
HALLMARK_DNA_REPAIR	146	-1.87	0.001	0.005

c2.all.v7.0

NAME	SIZE	NES	NOM p-val	FDR q-val
DUTERTRE_ESTRADIOL_RESPONSE_24HR_UP	303	-3.23	0.000	0.000
KOBAYASHI_EGFR_SIGNALING_24HR_DN	244	-3.08	0.000	0.000
ROSTY_CERVICAL_CANCER_PROLIFERATION_CLUSTER	135	-2.96	0.000	0.000
FUJII_YBX1_TARGETS_DN	187	-2.95	0.000	0.000
BURTON_ADIPOGENESIS_3	96	-2.93	0.000	0.000
VERNELL_RETINOBLASTOMA_PATHWAY_UP	69	-2.91	0.000	0.000
PUJANA_XPRSS_INT_NETWORK	161	-2.89	0.000	0.000
BLUM_RESPONSE_TO_SALIRASIB_DN	320	-2.89	0.000	0.000
GRAHAM_NORMAL_QUIESCENT_VS_NORMAL_DIVIDING_DN	85	-2.88	0.000	0.000
RUIZ_TNC_TARGETS_DN	140	-2.87	0.000	0.000
WHITEFORD_PEDIATRIC_CANCER_MARKERS	111	-2.86	0.000	0.000
ZHOU_CELL_CYCLE_GENES_IN_IR_RESPONSE_6HR	79	-2.86	0.000	0.000
PUJANA_BRCA2_PCC_NETWORK	403	-2.84	0.000	0.000
SHEDDEN_LUNG_CANCER_POOR_SURVIVAL_A6	428	-2.83	0.000	0.000
MISSIAGLIA_REGULATED_BY_METHYLATION_DN	115	-2.82	0.000	0.000
WHITFIELD_CELL_CYCLE_G1_S	125	-2.81	0.000	0.000
PUJANA_BRCA_CENTERED_NETWORK	116	-2.81	0.000	0.000
REACTOME_DNA_REPLICATION	123	-2.79	0.000	0.000
SOTIRIOU_BREAST_CANCER_GRADE_1_VS_3_UP	147	-2.79	0.000	0.000
SARRIO_EPITHELIAL_MESENCHYMAL_TRANSITION_UP	175	-2.78	0.000	0.000
CROONQUIST_IL6_DEPRIVATION_DN	93	-2.78	0.000	0.000
ZHOU_CELL_CYCLE_GENES_IN_IR_RESPONSE_24HR	116	-2.77	0.000	0.000
LEE_EARLY_T_LYMPHOCYTE_UP	99	-2.77	0.000	0.000
FISCHER_G1_S_CELL_CYCLE	188	-2.76	0.000	0.000
WINNEPENNINCKX_MELANOMA_METASTASIS_UP	156	-2.76	0.000	0.000
GRAHAM_CML_DIVIDING_VS_NORMAL_QUIESCENT_UP	169	-2.76	0.000	0.000

WANG_RESPONSE_TO_GSK3_INHIBITOR_SB216763_DN	336	-2.75	0.000	0.000
KONG_E2F3_TARGETS	91	-2.75	0.000	0.000
CHICAS_RB1_TARGETS_SENESCENT	488	-2.73	0.000	0.000
CROONQUIST_NRAS_SIGNALING_DN	69	-2.71	0.000	0.000
SONG_TARGETS_OF_IE86_CMV_PROTEIN	54	-2.70	0.000	0.000
KAUFFMANN_MELANOMA_RELAPSE_UP	61	-2.69	0.000	0.000
BENPORATH_PROLIFERATION	140	-2.69	0.000	0.000
REACTOME_DNA_REPLICATION_PRE_INITIATION	82	-2.68	0.000	0.000
REACTOME_DNA_STRAND_ELONGATION	32	-2.68	0.000	0.000
MANALO_HYPOXIA_DN	283	-2.68	0.000	0.000
REACTOME_MITOTIC_G1_G1_S_PHASES	145	-2.67	0.000	0.000
FLORIO_NEOCORTEX_BASAL_RADIAL_GLIA_DN	166	-2.66	0.000	0.000
REACTOME_S_PHASE	156	-2.66	0.000	0.000
REACTOME_ACTIVATION_OF_ATR_IN_RESPONSE_TO_REPLICATION_STRESS	37	-2.66	0.000	0.000
MARKEY_RB1_ACUTE_LOF_UP	214	-2.65	0.000	0.000
CHICAS_RB1_TARGETS_GROWING	214	-2.65	0.000	0.000
CHIANG_LIVER_CANCER_SUBCLASS_PROLIFERATION_UP	163	-2.64	0.000	0.000
STEIN_ESRRA_TARGETS_RESPONSIVE_TO_ESTROGEN_DN	39	-2.63	0.000	0.000
BILD_E2F3_ONCOGENIC_SIGNATURE	223	-2.63	0.000	0.000
KEGG_DNA_REPLICATION	36	-2.62	0.000	0.000
BERENJENO_TRANSFORMED_BY_RHOA_UP	497	-2.62	0.000	0.000
KAUFFMANN_DNA_REPLICATION_GENES	139	-2.62	0.000	0.000
HOFFMANN_LARGE_TO_SMALL_PRE_BII_LYMPHOCYTE_UP	142	-2.61	0.000	0.000
LINDGREN_BLADDER_CANCER_CLUSTER_3_UP	306	-2.61	0.000	0.000
REACTOME_HDR_THROUGH_HOMOLOGOUS_RECOMBINATION_HRR	64	-2.61	0.000	0.000
MORI_LARGE_PRE_BII_LYMPHOCYTE_UP	81	-2.60	0.000	0.000
LE_EGR2_TARGETS_UP	101	-2.60	0.000	0.000
TOYOTA_TARGETS_OF_MIR34B_AND_MIR34C	417	-2.60	0.000	0.000
REACTOME_ACTIVATION_OF_THE_PRE_REPLICATIVE_COMPLEX	33	-2.59	0.000	0.000
ISHIDA_E2F_TARGETS	50	-2.59	0.000	0.000
MORI_IMMATURE_B_LYMPHOCYTE_DN	86	-2.59	0.000	0.000
KANG_DOXORUBICIN_RESISTANCE_UP	52	-2.59	0.000	0.000
VECCHI_GASTRIC_CANCER_EARLY_UP	388	-2.59	0.000	0.000
WONG_EMBRYONIC_STEM_CELL_CORE	325	-2.58	0.000	0.000
DUTERTRE_ESTRADIOL_RESPONSE_6HR_UP	214	-2.58	0.000	0.000
PYEON_HPV_POSITIVE_TUMORS_UP	86	-2.58	0.000	0.000
REACTOME_HOMOLOGOUS_DNA_PAIRING_AND_STRAND_EXCHANGE	41	-2.57	0.000	0.000
PYEON_CANCER_HEAD_AND_NECK_VS_CERVICAL_UP	177	-2.56	0.000	0.000
LI_WILMS_TUMOR_VS_FETAL_KIDNEY_1_DN	155	-2.56	0.000	0.000
MITSIADES_RESPONSE_TO_APLIDIN_DN	241	-2.55	0.000	0.000
MOLENAAR_TARGETS_OF_CCND1_AND_CDK4_DN	52	-2.55	0.000	0.000
REACTOME_EXTENSION_OF_TELOMERES	30	-2.55	0.000	0.000

MUELLER_PLURINET	286	-2.54	0.000	0.000
WHITFIELD_CELL_CYCLE_S	143	-2.52	0.000	0.000
PUJANA_BREAST_CANCER_WITH_BRCA1_MUTATED_UP	54	-2.52	0.000	0.000
SENGUPTA_NASOPHARYNGEAL_CARCINOMA_UP	276	-2.52	0.000	0.000
GARCIA_TARGETS_OF_FLI1_AND_DAX1_DN	150	-2.52	0.000	0.000
REN_BOUND_BY_E2F	60	-2.51	0.000	0.000
FOURNIER_ACINAR_DEVELOPMENT_LATE_2	273	-2.51	0.000	0.000
STEIN_ESR1_TARGETS	73	-2.51	0.000	0.000
PID_FANCONI_PATHWAY	45	-2.50	0.000	0.000
BURTON_ADIPOGENESIS_PEAK_AT_16HR	38	-2.50	0.000	0.000
REACTOME_MITOTIC_PROMETAPHASE	191	-2.50	0.000	0.000
FRASOR_RESPONSE_TO_SERM_OR_FULVESTRANT_DN	45	-2.50	0.000	0.000
AFFAR_YY1_TARGETS_DN	197	-2.50	0.000	0.000
REACTOME_HDR_THROUGH_SINGLE_STRAND_ANNEALING_SSA	36	-2.50	0.000	0.000
ZHENG_GLIOBLASTOMA_PLASTICITY_UP	209	-2.49	0.000	0.000
KAUFFMANN_DNA_REPAIR_GENES	225	-2.45	0.000	0.000
PID_ATR_PATHWAY	39	-2.45	0.000	0.000
KAMMINGA_EZH2_TARGETS	41	-2.44	0.000	0.000
ZHAN_MULTIPLE_MYELOMA_PR_UP	43	-2.43	0.000	0.000
REACTOME_G1_S_SPECIFIC_TRANSCRIPTION	28	-2.43	0.000	0.000
REACTOME_TELOMERE_C_STRAND_LAGGING_STRAND_SYNTHESIS	24	-2.42	0.000	0.000
MARKEY_RB1_CHRONIC_LOF_UP	98	-2.41	0.000	0.000
BASAKI_YBX1_TARGETS_UP	268	-2.41	0.000	0.000
BENPORATH_ES_1	341	-2.41	0.000	0.000
MORI_PRE_BI_LYMPHOCYTE_UP	74	-2.41	0.000	0.000
VANTVEER_BREAST_CANCER_METASTASIS_DN	119	-2.41	0.000	0.000
RHEIN_ALL_GLUCOCORTICOID_THERAPY_DN	350	-2.40	0.000	0.000
EGUCHI_CELL_CYCLE_RB1_TARGETS	23	-2.39	0.000	0.000
ODONNELL_TARGETS_OF_MYC_AND_TFRC_DN	43	-2.39	0.000	0.000
RHODES_UNDIFFERENTIATED_CANCER	66	-2.39	0.000	0.000
REACTOME_CELL_CYCLE_CHECKPOINTS	267	-2.38	0.000	0.000
REACTOME_RECOGNITION_OF_DNA_DAMAGE_BY_PCNA_CONTAINING_REPLICATION_COMPLEX	30	-2.38	0.000	0.000
FURUKAWA_DUSP6_TARGETS_PCI35_DN	63	-2.37	0.000	0.000
FERRANDO_T_ALL_WITH_MLL_ENL_FUSION_DN	77	-2.37	0.000	0.000
REACTOME_DNA_DAMAGE_BYPASS	45	-2.36	0.000	0.000
REACTOME_RESOLUTION_OF_ABASIC_SITES_AP_SITES	38	-2.36	0.000	0.000
MORI_EMU_MYC_LYMPHOMA_BY_ONSET_TIME_UP	102	-2.36	0.000	0.000
ODONNELL_TFRC_TARGETS_DN	120	-2.35	0.000	0.000
VILLANUEVA_LIVER_CANCER_KRT19_UP	164	-2.35	0.000	0.000
REACTOME_RESOLUTION_OF_SISTER_CHROMATID_COHESION	118	-2.35	0.000	0.000
PID_E2F_PATHWAY	68	-2.35	0.000	0.000

RIZ_ERYTHROID_DIFFERENTIATION	78	-2.35	0.000	0.000
WHITFIELD_CELL_CYCLE_LITERATURE	41	-2.34	0.000	0.000
HORIUCHI_WTAP_TARGETS_DN	294	-2.34	0.000	0.000
REACTOME_ASSEMBLY_OF_THE_PRE_REPLICATIVE_COMPLEX	65	-2.34	0.000	0.000
REACTOME_GAP_FILLING_DNA_REPAIR_SYNTHESIS_AND_LIGATION_IN_GG_NER	25	-2.34	0.000	0.000
FERREIRA_EWINGS_SARCOMA_UNSTABLE_VS_STABLE_UP	148	-2.34	0.000	0.000
GOLDRATH_ANTIGEN_RESPONSE	316	-2.32	0.000	0.000
REACTOME_RESOLUTION_OF_AP_SITES_VIA_THE_MULTIPLE_NUCLEOTIDE_PATCH _REPLACEMENT_PATHWAY	25	-2.32	0.000	0.000
PUJANA_BREAST_CANCER_LIT_INT_NETWORK	98	-2.31	0.000	0.000
REACTOME_PCNA_DEPENDENT_LONG_PATCH_BASE_EXCISION_REPAIR	21	-2.31	0.000	0.000
SUNG_METASTASIS_STROMA_DN	47	-2.30	0.000	0.000
REACTOME_LAGGING_STRAND_SYNTHESIS	20	-2.30	0.000	0.000

Supplementary Table S5.

Significantly upregulated gene sets in MM.1S cells treated with combination treatment of PTC596 with bortezomib.

Gene set enrichment analysis using our RNA-seq data identified gene sets, which were significantly enriched in MM.1S cells treated with the combination treatment versus control. (FDR w-value <0.01).

Hallmark

NAME	SIZE	NES	NOM p-val	FDR q-val
HALLMARK_TNFA_SIGNALING_VIA_NFKB	183	2.31	0.000	0.000
HALLMARK_APOPTOSIS	152	2.12	0.000	0.000
HALLMARK_P53_PATHWAY	187	1.98	0.000	0.000
HALLMARK_HYPOXIA	182	1.88	0.000	0.000
HALLMARK_UV_RESPONSE_UP	148	1.71	0.000	0.006
HALLMARK_IL6_JAK_STAT3_SIGNALING	68	1.64	0.000	0.008
HALLMARK_REACTIVE_OXYGEN_SPECIES_PATHWAY	46	1.63	0.002	0.007
HALLMARK_UNFOLDED_PROTEIN_RESPONSE	109	1.60	0.000	0.008
HALLMARK_HEME_METABOLISM	176	1.60	0.000	0.007

c2.all.v7.0

NAME	SIZE	NES	NOM p-val	FDR q-val
PODAR_RESPONSE_TO_ADAPHOSTIN_UP	144	3.01	0.000	0.000
CONCANNON_APOPTOSIS_BY_EPOXOMICIN_UP	224	2.93	0.000	0.000
GARGALOVIC_RESPONSE_TO_OXIDIZED_PHOSPHOLIPIDS_BLUE_UP	128	2.70	0.000	0.000
REACTOME_HSP90_CHAPERONE_CYCLE_FOR_STEROID_HORMONE_RECEPTORS_SHR	54	2.52	0.000	0.000
REACTOME_THE_ROLE_OF_GTSE1_IN_G2_M_PROGRESSION_AFTER_G2_CHECKPOINT	74	2.51	0.000	0.000
REACTOME_AUF1_HNRNP_D0_BINDS_AND_DESTABILIZES_MRNA	52	2.49	0.000	0.000
REACTOME_DECTIN_1_MEDIATED_NONCANONICAL_NF_KB_SIGNALING	58	2.45	0.000	0.000
REACTOME_STABILIZATION_OF_P53	53	2.44	0.000	0.000
REACTOME_HSF1_DEPENDENT_TRANSACTIVATION	35	2.42	0.000	0.000
REACTOME_HEDGEHOG_LIGAND_BIOGENESIS	59	2.41	0.000	0.000
PICCALUGA_ANGIOIMMUNOBLASTIC_LYMPHOMA_DN	130	2.40	0.000	0.000
REACTOME_VIF_MEDIATED_DEGRADATION_OF_APOBEC3G	49	2.40	0.000	0.000
REACTOME_DEGRADATION_OF_AXIN	52	2.40	0.000	0.000
REACTOME_ABC_TRANSPORTER_DISORDERS	71	2.40	0.000	0.000
REACTOME_FCERI_MEDIATED_NF_KB_ACTIVATION	78	2.39	0.000	0.000
REACTOME_NEGATIVE_REGULATION_OF_NOTCH4_SIGNALING	53	2.38	0.000	0.000
KEGG_PROTEASOME	41	2.37	0.000	0.000
REACTOME_DEGRADATION_OF_GLI1_BY_THE_PROTEASOME	57	2.36	0.000	0.000
REACTOME_ACTIVATION_OF_NF_KAPPAB_IN_B_CELLS	64	2.36	0.000	0.000
REACTOME_CROSS_PRESENTATION_OF_SOLUBLE_EXOGENOUS_ANTIGENS_ENDOSOMES	43	2.36	0.000	0.000

REACTOME_MAPK6_MAPK4_SIGNALING	83	2.35	0.000	0.000
REACTOME_FBXL7_DOWN_REGULATES_AURKA_DURING_MITOTIC_ENTRY_AND_IN_EAR	52	2.35	0.000	0.000
LY_MITOSIS				
REACTOME_REGULATION_OF_PTEN_STABILITY_AND_ACTIVITY	65	2.35	0.000	0.000
REACTOME_REGULATION_OF_APOPTOSIS	50	2.35	0.000	0.000
REACTOME_CELLULAR_RESPONSE_TO_HYPOXIA	68	2.35	0.000	0.000
REACTOME_ATTENUATION_PHASE	26	2.35	0.000	0.000
GARGALOVIC_RESPONSE_TO_OXIDIZED_PHOSPHOLIPIDS_TURQUOISE_UP	76	2.34	0.000	0.000
REACTOME_INTERLEUKIN_1_SIGNALING	95	2.34	0.000	0.000
REACTOME_DEGRADATION_OF_DVL	54	2.33	0.000	0.000
REACTOME_ABC_FAMILY_PROTEINS_MEDIATED_TRANSPORT	95	2.33	0.000	0.000
REACTOME_DEFECTIVE_CFTR_CAUSES_CYSTIC_FIBROSIS	57	2.33	0.000	0.000
REACTOME_CLEC7A_DECTIN_1_SIGNALING	95	2.33	0.000	0.000
REACTOME_REGULATION_OF_MRNA_STABILITY_BY_	84	2.32	0.000	0.000
PROTEINS_THAT_BIND_AU_RICH_ELEMENTS				
REACTOME_REGULATION_OF_RUNX3_EXPRESSION_AND_ACTIVITY	54	2.31	0.000	0.000
NOJIMA_SFRP2_TARGETS_UP	30	2.30	0.000	0.000
REACTOME_ANTIGEN_PROCESSING_CROSS_PRESENTATION	92	2.29	0.000	0.000
REACTOME_METABOLISM_OF_POLYAMINES	56	2.29	0.000	0.000
REACTOME_HSF1_ACTIVATION	29	2.28	0.000	0.000
REACTOME_TNFR2_NON_CANONICAL_NF_KB_PATHWAY	89	2.27	0.000	0.000
REACTOME_REGULATION_OF_RUNX2_EXPRESSION_AND_ACTIVITY	68	2.26	0.000	0.000
GERY_CEBP_TARGETS	104	2.25	0.000	0.000
BLUM_RESPONSE_TO_SALIRASIB_UP	235	2.24	0.000	0.000
REACTOME_DEGRADATION_OF_BETA_CATENIN_BY_THE_DESTRUCTION_COMPLEX	79	2.24	0.000	0.000
REACTOME_DOWNSTREAM_SIGNALING_EVENTS_OF_B_CELL_RECEPTOR_BCR	78	2.22	0.000	0.000
GARGALOVIC_RESPONSE_TO_OXIDIZED_PHOSPHOLIPIDS_MAGENTA_UP	27	2.22	0.000	0.000
REACTOME_G1_S_DNA_DAMAGE_CHECKPOINTS	63	2.21	0.000	0.000
REACTOME_HEDGEHOG_OFF_STATE	105	2.21	0.000	0.000
REACTOME_COPI_INDEPENDENT_GOLGI_TO_ER_RETROGRADE_TRAFFIC	50	2.21	0.000	0.000
KRIGE_AMINO_ACID_DEPRIVATION	27	2.21	0.000	0.000
HELLER_SILENCED_BY_METHYLATION_DN	102	2.20	0.000	0.000
REACTOME_REGULATION_OF_EXPRESSION_OF_SLITS_AND_ROBOS	158	2.20	0.000	0.000
LEONARD_HYPOXIA	42	2.20	0.000	0.000
TIEN_INTESTINE_PROBIOTICS_24HR_DN	201	2.19	0.000	0.000
REACTOME_SIGNALING_BY_NOTCH4	81	2.19	0.000	0.000
REACTOME_HEDGEHOG_ON_STATE	80	2.18	0.000	0.000
GALINDO_IMMUNE_RESPONSE_TO_ENTEROTOXIN	71	2.18	0.000	0.000
REACTOME_CELLULAR_RESPONSE_TO_HEAT_STRESS	96	2.18	0.000	0.000
BURTON_ADIPOGENESIS_PEAK_AT_2HR	39	2.17	0.000	0.000
REACTOME_C_TYPE_LECTIN_RECEPTORS_CLRS	124	2.16	0.000	0.000
KAN_RESPONSE_TO_ARSENIC_TRIOXIDE	99	2.16	0.000	0.000

REACTOME_UCH_PROTEINASES	96	2.15	0.000	0.000
CHEN_LVAD_SUPPORT_OF_FAILING_HEART_UP	82	2.15	0.000	0.000
REACTOME_DOWNSTREAM_TCR_SIGNALING	88	2.15	0.000	0.000
MITSIADES_RESPONSE_TO_APLIDIN_UP	423	2.15	0.000	0.000
NAGASHIMA_NRG1_SIGNALING_UP	157	2.14	0.000	0.000
REACTOME_SIGNALING_BY_HEDGEHOG	138	2.14	0.000	0.000
CHEN_HOXA5_TARGETS_9HR_UP	210	2.13	0.000	0.000
REACTOME_TRANSCRIPTIONAL_REGULATION_BY_RUNX3	93	2.13	0.000	0.000
REACTOME_ASYMMETRIC_LOCALIZATION_OF_PCP_PROTEINS	61	2.13	0.000	0.000
GROSS_HYPOXIA_VIA_ELK3_DN	133	2.13	0.000	0.000
CHO_NR4A1_TARGETS	24	2.13	0.000	0.000
CHUANG_OXIDATIVE_STRESS_RESPONSE_UP	26	2.12	0.000	0.000
REACTOME_EUKARYOTIC_TRANSLATION_INITIATION	114	2.12	0.000	0.000
DANG_MYC_TARGETS_DN	29	2.12	0.000	0.000
REACTOME_SCF_SKP2_MEDIATED_DEGRADATION_OF_P27_21	58	2.11	0.000	0.000
HOUSTIS_ROS	31	2.11	0.000	0.000
REACTOME_REGULATION_OF_RAS_BY_GAPS	65	2.11	0.000	0.000
AMUNDSON_RESPONSE_TO_ARSENITE	205	2.11	0.000	0.000
DALESSIO_TSA_RESPONSE	18	2.10	0.000	0.000
CHIBA_RESPONSE_TO_TSA	38	2.10	0.000	0.000
DIRMEIER_LMP1_RESPONSE_EARLY	59	2.10	0.000	0.000
REACTOME_APC_C:CDH1_MEDIATED_DEGRADATION_OF_CDC20_AND_OTHER_APC_C:CDH1_TARGETED_PROTEINS_IN_LATE_MITOSIS_EARLY_G1	69	2.09	0.000	0.000
KEGG_RIBOSOME	82	2.08	0.000	0.000
REACTOME_CELLULAR_RESPONSES_TO_EXTERNAL_STIMULI	479	2.08	0.000	0.000
REACTOME_INTERLEUKIN_1_FAMILY_SIGNALING	121	2.08	0.000	0.000
REACTOME_CELLULAR_RESPONSES_TO_STRESS	396	2.08	0.000	0.000
HARRIS_HYPOXIA	67	2.07	0.000	0.000
REACTOME_ACTIVATION_OF_APC_C_AND_APC_C:CDC20_MEDIATED_DEGRADATION_OF_MITOTIC_PROTEINS	72	2.06	0.000	0.000
REACTOME_ANTIGEN_PROCESSING:_UBIQUITINATION_PROTEASOME_DEGRADATION	284	2.05	0.000	0.000
SMIRNOV_RESPONSE_TO_IR_2HR_UP	51	2.05	0.000	0.000
WONG_PROTEASOME_GENE_MODULE	50	2.03	0.000	0.001
REACTOME_CDK_MEDIATED_PHOSPHORYLATION_AND_REMOVAL_OF_CDC6	68	2.03	0.000	0.001
REACTOME_CLASS_I_MHC_MEDIATED_ANTIGEN_PROCESSING_PRESENTATION	342	2.03	0.000	0.001
REACTOME_CARBOXYTERMINAL_POST_TRANSLATIONAL_MODIFICATIONS_OF_TUBULIN	34	2.03	0.000	0.001
SESTO_RESPONSE_TO_UV_C0	99	2.03	0.000	0.001
REACTOME_FC_EPSILON_RECEPTOR_FCERI_SIGNALING	127	2.03	0.000	0.001
NAGASHIMA_EGF_SIGNALING_UP	51	2.02	0.000	0.001
AMIT_EGF_RESPONSE_40_HELA	38	2.02	0.000	0.001
REACTOME_DISORDERS_OF_TRANSMEMBRANE_TRANSPORTERS	152	2.01	0.000	0.001
REACTOME_ASSEMBLY_AND_CELL_SURFACE_PRESENTATION_OF_NMDA_RECEPTORS	39	2.01	0.000	0.001

KRIEG_HYPOXIA_VIA_KDM3A	46	2.01	0.000	0.001
UDAYAKUMAR_MED1_TARGETS_DN	224	2.01	0.000	0.001
SUH_COEXPRESSED_WITH_ID1_AND_ID2_UP	16	2.00	0.000	0.001
WINTER_HYPOXIA_METAGENE	208	2.00	0.000	0.001
REACTOME_UB_SPECIFIC_PROCESSING_PROTEASES	183	2.00	0.000	0.001
REACTOME_TCR_SIGNALING	107	2.00	0.000	0.001
GRAHAM_CML_QUIESCENT_VS_NORMAL_DIVIDING_UP	44	1.99	0.000	0.001
REACTOME_NONSENSE_MEDIATED_DECAY_NMD_INDEPENDENT_OF_THE_EXON_JUNCTION_COMPLEX_EJC	90	1.99	0.000	0.001
RASHI_RESPONSE_TO_IONIZING_RADIATION_1	36	1.98	0.000	0.001
REACTOME_GAP_JUNCTION_ASSEMBLY	26	1.98	0.000	0.001
REACTOME_AUTOPHAGY	104	1.98	0.000	0.001
REACTOME_REGULATION_OF_HSF1_MEDIATED_HEAT_SHOCK_RESPONSE	78	1.98	0.000	0.001
MARKEY_RB1_CHRONIC_LOF_DN	95	1.98	0.000	0.001
GARGALOVIC_RESPONSE_TO_OXIDIZED_PHOSPHOLIPIDS_YELLOW_UP	30	1.97	0.000	0.001
DAZARD_UV_RESPONSE_CLUSTER_G4	16	1.97	0.000	0.001
APPIERTO_RESPONSE_TO_FENRETINIDE_UP	31	1.97	0.000	0.001
KIM_WT1_TARGETS_8HR_UP	154	1.96	0.000	0.002
NAKAYAMA_FRA2_TARGETS	40	1.96	0.000	0.002
REACTOME_TRANSPORT_OF_CONNEXONS_TO_THE_PLASMA_MEMBRANE	19	1.96	0.000	0.002
PID_FRA_PATHWAY	31	1.96	0.000	0.002
RHEIN_ALL_GLUCOCORTICOID_THERAPY_UP	61	1.95	0.000	0.002
REACTOME_PCP_CE_PATHWAY	87	1.95	0.000	0.002
YAO_TEMPORAL_RESPONSE_TO_PROGESTERONE_CLUSTER_1	56	1.95	0.002	0.002
YAN_ESCAPE_FROM_ANOIKIS	20	1.95	0.000	0.002
REACTOME_PROGRAMMED_CELL_DEATH	166	1.95	0.000	0.002
REACTOME_REGULATED_NECROSIS	20	1.95	0.000	0.002
REACTOME_CYCLIN_A:CDK2_ASSOCIATED_EVENTS_AT_S_PHASE_ENTRY	83	1.95	0.000	0.002
DORSAM_HOXA9_TARGETS_DN	29	1.95	0.000	0.002
REACTOME_REGULATION_OF_MITOTIC_CELL_CYCLE	82	1.94	0.000	0.002
REACTOME_COPI_MEDIATED_ANTEROGRADE_TRANSPORT	97	1.94	0.000	0.002
REACTOME_MITOPHAGY	26	1.94	0.000	0.002
REACTOME_INTERLEUKIN_4_AND_INTERLEUKIN_13_SIGNALING	87	1.94	0.000	0.002
DAZARD_UV_RESPONSE_CLUSTER_G24	16	1.94	0.002	0.002
REACTOME_SIGNALING_BY_ROBO_RECEPTORS	202	1.93	0.000	0.002
DEN_INTERACT_WITH_LCA5	25	1.93	0.002	0.002
REACTOME_IRON_UPTAKE_AND_TRANSPORT	53	1.92	0.000	0.003
REACTOME_DEUBIQUITINATION	255	1.92	0.000	0.003
ZHANG_RESPONSE_TO_IKK_INHIBITOR_AND_TNF_UP	194	1.92	0.000	0.003
REACTOME_NONSENSE_MEDIATED_DECAY_NMD	110	1.92	0.000	0.003
REACTOME_TRANSCRIPTIONAL_REGULATION_BY_RUNX2	108	1.92	0.000	0.003
SARRIO_EPITHELIAL_MESENCHYMAL_TRANSITION_DN	129	1.92	0.000	0.003

REACTOME_SIGNALING_BY_THE_B_CELL_RECEPTOR_BCR	105	1.92	0.000	0.003
BILANGES_SERUM_AND_RAPAMYCIN_SENSITIVE_GENES	46	1.92	0.000	0.003
DAUER_STAT3_TARGETS_UP	39	1.92	0.002	0.003
AMIT_DELAYED_EARLY_GENES	18	1.92	0.000	0.003
DEBIASI_APOPTOSIS_BY_REOVIRUS_INFECTION_UP	275	1.91	0.000	0.003
REACTOME_RUNX1_REGULATES_TRANSCRIPTION_OF_GENES_INVOLVED_IN_DIFFEREN	108	1.91	0.000	0.003
TIATION_OF_HSCS				
AMIT_SERUM_RESPONSE_120_MCF10A	65	1.91	0.000	0.003
AMIT_SERUM_RESPONSE_40_MCF10A	29	1.90	0.000	0.003
REACTOME_PINK_PARKIN_MEDIATED_MITOPHAGY	19	1.90	0.000	0.003
AMIT_EGF_RESPONSE_60_HELA	41	1.90	0.000	0.003
WENG_POR_DOSAGE	15	1.90	0.000	0.003
REACTOME_ACTIVATION_OF_THE_MRNA_UPON_BINDING_OF_THE_CAP_BINDING_COMP	57	1.90	0.000	0.003
LEX_AND_EIFS_AND_SUBSEQUENT_BINDING_TO_43S				
FALVELLA_SMOKERS_WITH_LUNG_CANCER	70	1.90	0.000	0.003
REACTOME_PTEN_REGULATION	132	1.90	0.000	0.003
ABRAHAM_ALPC_VS_MULTIPLE_MYELOMA_UP	22	1.90	0.002	0.003
VARELA_ZMPSTE24_TARGETS_UP	40	1.90	0.000	0.003
REACTOME_ASSEMBLY_OF_THE_PRE_REPLICATIVE_COMPLEX	65	1.90	0.000	0.003
MCDOWELL_ACUTE_LUNG_INJURY_UP	37	1.89	0.000	0.004
REACTOME_MITOTIC_G2_G2_M_PHASES	193	1.89	0.000	0.004
REACTOME_ORC1_REMOVAL_FROM_CHROMATIN	67	1.89	0.000	0.004
GENTILE_UV_HIGH_DOSE_UP	18	1.89	0.000	0.004
REACTOME_HOST_INTERACTIONS_OF_HIV_FACTORS	121	1.88	0.000	0.004
REACTOME_MAP3K8_TPL2_DEPENDENT_MAPK1_3_ACTIVATION	16	1.88	0.000	0.004
SEMENZA_HIF1_TARGETS	33	1.88	0.000	0.004
BAKKER_FOXO3_TARGETS_UP	50	1.87	0.002	0.005
ZWANG_CLASS_2_TRANSIENTLY_INDUCED_BY_EGF	38	1.87	0.000	0.005
LIAN_LIPA_TARGETS_6M	51	1.87	0.000	0.005
ENK_UV_RESPONSE_KERATINOCYTE_UP	458	1.87	0.000	0.005
REACTOME_POST_CHAPERONIN_TUBULIN_FOLDING_PATHWAY	22	1.87	0.004	0.005
CAFFAREL_RESPONSE_TO_THC_UP	32	1.87	0.000	0.005
HAN_JNK_SINGALING_UP	29	1.86	0.000	0.005
REACTOME_INFECTIOUS_DISEASE	356	1.86	0.000	0.005
GRAHAM_NORMAL_QUIESCENT_VS_NORMAL_DIVIDING_UP	49	1.86	0.000	0.005
PRAMOONJAGO_SOX4_TARGETS_UP	49	1.86	0.000	0.006
LIAN_LIPA_TARGETS_3M	42	1.86	0.000	0.006
ODONNELL_TARGETS_OF_MYC_AND_TFRC_UP	71	1.86	0.000	0.006
REACTOME_GAP_JUNCTION_TRAFFICKING_AND_REGULATION	39	1.85	0.000	0.006
REACTOME_FORMATION_OF_TUBULIN_FOLDING_INTERMEDIATES_BY_CCT_TRIC	25	1.85	0.002	0.006
LAMB_CCND1_TARGETS	17	1.85	0.000	0.006
FERRARI_RESPONSE_TO_FENRETINIDE_UP	20	1.84	0.000	0.007

REACTOME_MACROAUTOPHAGY	86	1.84	0.000	0.007
REACTOME_NEDDYLATION	219	1.84	0.000	0.007
MISSIAGLIA_REGULATED_BY_METHYLATION_UP	108	1.83	0.000	0.007
GARGALOVIC_RESPONSE_TO_OXIDIZED_PHOSPHOLIPIDS_GREY_UP	17	1.83	0.006	0.008
PETROVA_ENDOTHELIUM_LYMPHATIC_VS_BLOOD_DN	138	1.83	0.000	0.008
RASHI_RESPONSE_TO_IONIZING_RADIATION_2	103	1.83	0.000	0.008
REACTOME_GOLGI_TO_ER_RETROGRADE_TRANSPORT	125	1.83	0.000	0.008
REACTOME_ACTIVATION_OF_AMPK_DOWNSTREAM_OF_NMDARS	26	1.83	0.000	0.008
TIAN_TNF_SIGNALING_NOT_VIA_NFKB	22	1.82	0.002	0.008
PHONG_TNF_TARGETS_UP	58	1.82	0.000	0.009
ZWANG_CLASS_1_TRANSIENTLY_INDUCED_BY_EGF	434	1.82	0.000	0.009
WIERENGA_STAT5A_TARGETS_GROUP2	45	1.82	0.000	0.009
KIM_WT1_TARGETS_12HR_UP	146	1.81	0.000	0.009
PELLICCIOTTA_HDAC_IN_ANTIGEN_PRESENTATION_UP	59	1.81	0.000	0.009
REACTOME_INFLUENZA_INFECTION	147	1.81	0.000	0.010
REACTOME_MITOTIC_METAPHASE_AND_ANAPHASE	191	1.81	0.000	0.010
GROSS_HYPOXIA_VIA_ELK3_ONLY_UP	25	1.81	0.002	0.010

Supplementary Table S6.

Significantly downregulated gene sets in MM.1S cells treated with combination treatment of PTC596 with bortezomib.

Gene set enrichment analysis using our RNA-seq data identified gene sets, which were significantly downregulated in MM.1S cells treated with the combination treatment versus control. (FDR w-value <0.01).

Hallmark

NAME	SIZE	NES	NOM p-val	FDR q-val
HALLMARK_E2F_TARGETS	196	-2.48	0.000	0.000
HALLMARK_G2M_CHECKPOINT	189	-1.88	0.000	0.001
HALLMARK_CHOLESTEROL_HOMEOSTASIS	72	-1.73	0.004	0.007

c2.all.v7.0

NAME	SIZE	NES	NOM p-val	FDR q-val
DUTERTRE_ESTRADIOL_RESPONSE_24HR_UP	303	-2.64	0.000	0.000
ROSTY_CERVICAL_CANCER_PROLIFERATION_CLUSTER	135	-2.55	0.000	0.000
VERNELL_RETINOBLASTOMA_PATHWAY_UP	69	-2.52	0.000	0.000
CONCANNON_APOPTOSIS_BY_EPOXOMICIN_DN	156	-2.49	0.000	0.000
ZHOU_CELL_CYCLE_GENES_IN_IR_RESPONSE_6HR	79	-2.49	0.000	0.000
MISSIAGLIA_REGULATED_BY_METHYLATION_DN	115	-2.42	0.000	0.000
GRAHAM_NORMAL_QUIESCENT_VS_NORMAL_DIVIDING_DN	85	-2.42	0.000	0.000
GRAHAM_CML_DIVIDING_VS_NORMAL_QUIESCENT_UP	169	-2.42	0.000	0.000
RUIZ_TNC_TARGETS_DN	140	-2.41	0.000	0.000
ZHOU_CELL_CYCLE_GENES_IN_IR_RESPONSE_24HR	116	-2.40	0.000	0.000
KOBAYASHI_EGFR_SIGNALING_24HR_DN	244	-2.37	0.000	0.000
ISHIDA_E2F_TARGETS	50	-2.36	0.000	0.000
SONG_TARGETS_OF_IE86_CMV_PROTEIN	54	-2.36	0.000	0.000
BURTON_ADIPOGENESIS_3	96	-2.34	0.000	0.000
FUJII_YBX1_TARGETS_DN	187	-2.33	0.000	0.000
REN_BOUND_BY_E2F	60	-2.32	0.000	0.000
ALCALAY_AML_BY_NPM1_LOCALIZATION_DN	169	-2.32	0.000	0.000
PUJANA_XPRSS_INT_NETWORK	161	-2.30	0.000	0.000
PUJANA_BRCA2_PCC_NETWORK	403	-2.30	0.000	0.000
PUJANA_BRCA_CENTERED_NETWORK	116	-2.26	0.000	0.000
WHITEFORD_PEDIATRIC_CANCER_MARKERS	111	-2.25	0.000	0.000
FISCHER_G1_S_CELL_CYCLE	188	-2.25	0.000	0.000
CROONQUIST_IL6_DEPRIVATION_DN	93	-2.23	0.000	0.000
REACTOME_DNA_STRAND_ELONGATION	32	-2.23	0.000	0.000
KAUFFMANN_MELANOMA_RELAPSE_UP	61	-2.22	0.000	0.000
BLUM_RESPONSE_TO_SALIRASIB_DN	320	-2.22	0.000	0.000
KEGG_DNA_REPLICATION	36	-2.20	0.000	0.000

AFFAR_YY1_TARGETS_DN	197	-2.20	0.000	0.000
SCHMIDT_POR_TARGETS_IN_LIMB_BUD_UP	24	-2.20	0.000	0.000
PYEON_HPV_POSITIVE_TUMORS_UP	86	-2.19	0.000	0.000
FOURNIER_ACINAR_DEVELOPMENT_LATE_2	273	-2.18	0.000	0.000
STEIN_ESRRA_TARGETS_RESPONSIVE_TO_ESTROGEN_DN	39	-2.18	0.000	0.000
SARRIO_EPITHELIAL_MESENCHYMAL_TRANSITION_UP	175	-2.17	0.000	0.000
CHICAS_RB1_TARGETS_GROWING	214	-2.16	0.000	0.000
KONG_E2F3_TARGETS	91	-2.15	0.000	0.000
REACTOME_CHOLESTEROL_BIOSYNTHESIS	24	-2.15	0.000	0.000
WENG_POR_TARGETS_GLOBAL_UP	16	-2.14	0.000	0.000
LEE_EARLY_T_LYMPHOCYTE_UP	99	-2.14	0.000	0.000
PUJANA_BREAST_CANCER_WITH_BRCA1_MUTATED_UP	54	-2.14	0.000	0.000
MARKEY_RB1_ACUTE_LOF_UP	214	-2.13	0.000	0.000
REACTOME_EXTENSION_OF_TELOMERES	30	-2.13	0.000	0.000
MITSIADES_RESPONSE_TO_APLIDIN_DN	241	-2.12	0.000	0.000
MARKEY_RB1_CHRONIC_LOF_UP	98	-2.11	0.000	0.000
CHICAS_RB1_TARGETS_SENESCENT	488	-2.10	0.000	0.000
BILD_E2F3_ONCOGENIC_SIGNATURE	223	-2.10	0.000	0.000
REACTOME_ACTIVATION_OF_THE_PRE_REPLICATIVE_COMPLEX	33	-2.09	0.000	0.000
REACTOME_ACTIVATION_OF_ATR_IN_RESPONSE_TO_REPLICATION_STR ESS	37	-2.09	0.000	0.000
MANALO_HYPOXIA_DN	283	-2.09	0.000	0.000
FRASOR_RESPONSE_TO_SERM_OR_FULVESTRANT_DN	45	-2.09	0.000	0.000
MORI_IMMATURE_B_LYMPHOCYTE_DN	86	-2.09	0.000	0.000
SCHUHMACHER_MYC_TARGETS_UP	78	-2.07	0.000	0.000
BENPORATH_ES_2	35	-2.07	0.000	0.000
MOLENAAR_TARGETS_OF_CCND1_AND_CDK4_DN	52	-2.07	0.000	0.000
CHIANG_LIVER_CANCER_SUBCLASS_PROLIFERATION_UP	163	-2.07	0.000	0.000
CUI_TCF21_TARGETS_2_UP	352	-2.07	0.000	0.000
KANG_DOXORUBICIN_RESISTANCE_UP	52	-2.06	0.000	0.000
CROONQUIST_NRAS_SIGNALING_DN	69	-2.06	0.000	0.000
REACTOME_HDR_THROUGH_SINGLE_STRAND_ANNEALING_SSA	36	-2.05	0.000	0.000
FERRANDO_HOX11_NEIGHBORS	17	-2.05	0.000	0.000
FLORIO_NEOCORTEX_BASAL_RADIAL_GLIA_DN	166	-2.05	0.000	0.000
WHITFIELD_CELL_CYCLE_LITERATURE	41	-2.05	0.000	0.000
MORI_EMU_MYC_LYMPHOMA_BY_ONSET_TIME_UP	102	-2.05	0.000	0.000
GAL_LEUKEMIC_STEM_CELL_DN	173	-2.05	0.000	0.000
LE_EGR2_TARGETS_UP	101	-2.05	0.000	0.000
SOTIRIOU_BREAST_CANCER_GRADE_1_VS_3_UP	147	-2.04	0.000	0.000
BURTON_ADIPOGENESIS_PEAK_AT_16HR	38	-2.04	0.000	0.000
KAMMINGA_EZH2_TARGETS	41	-2.04	0.000	0.000
EGUCHI_CELL_CYCLE_RB1_TARGETS	23	-2.04	0.000	0.000

SMID_BREAST_CANCER_RELAPSE_IN_BRAIN_UP	27	-2.03	0.000	0.000
SENGUPTA_NASOPHARYNGEAL_CARCINOMA_UP	276	-2.03	0.000	0.000
REACTOME_HOMOLOGOUS_DNA_PAIRING_AND_STRAND_EXCHANGE	41	-2.03	0.000	0.000
REACTOME_TELOMERE_C_STRAND_LAGGING_STRAND_SYNTHESIS	24	-2.03	0.000	0.000
SUNG_METASTASIS_STROMA_DN	47	-2.03	0.000	0.000
WHITFIELD_CELL_CYCLE_G1_S	125	-2.01	0.000	0.000
TAKEDA_TARGETS_OF_NUP98_HOXA9_FUSION_16D_UP	138	-2.01	0.000	0.000
GARGALOVIC_RESPONSE_TO_OXIDIZED_PHOSPHOLIPIDS_TURQUOISE_DN	53	-2.00	0.000	0.001
ZHAN_MULTIPLE_MYELOMA_PR_UP	43	-2.00	0.000	0.001
TORCHIA_TARGETS_OF_EWSR1_FLI1_FUSION_DN	271	-2.00	0.000	0.001
REACTOME_FATTY_ACYL_COA_BIOSYNTHESIS	34	-1.98	0.000	0.001
REACTOME_REGULATION_OF_CHOLESTEROL_BIOSYNTHESIS_BY_SREBP_SREBF	55	-1.98	0.000	0.001
REACTOME_ACTIVATION_OF_GENE_EXPRESSION_BY_SREBF_SREBP	42	-1.98	0.000	0.001
BOYAULT_LIVER_CANCER_SUBCLASS_G23_UP	52	-1.98	0.000	0.001
DUTERTRE_ESTRADIOL_RESPONSE_6HR_UP	214	-1.98	0.000	0.001
KEGG_BUTANOATE_METABOLISM	29	-1.98	0.000	0.001
ODONNELL_TFRC_TARGETS_DN	120	-1.97	0.000	0.001
STEIN_ESR1_TARGETS	73	-1.97	0.000	0.001
HORTON_SREBF_TARGETS	23	-1.97	0.000	0.001
YU_MYC_TARGETS_UP	40	-1.97	0.000	0.001
BENPORATH_ES_1	341	-1.97	0.000	0.001
HOFFMANN_LARGE_TO_SMALL_PRE_BII_LYMPHOCYTE_UP	142	-1.97	0.000	0.001
REACTOME_PCNA_DEPENDENT_LONG_PATCH_BASE_EXCISION_REPAIR	21	-1.95	0.002	0.001
VALK_AML_CLUSTER_10	24	-1.95	0.000	0.001
SHEDDEN_LUNG_CANCER_POOR_SURVIVAL_A6	428	-1.94	0.000	0.001
KEGG_BIOSYNTHESIS_OF_UNSATURATED_FATTY_ACIDS	18	-1.94	0.000	0.001
BIOCARTA_MCM_PATHWAY	18	-1.93	0.000	0.002
JAATINEN_HEMATOPOIETIC_STEM_CELL_UP	272	-1.93	0.000	0.002
BURTON_ADIPOGENESIS_PEAK_AT_24HR	38	-1.93	0.000	0.002
RHEIN_ALL_GLUCOCORTICOID_THERAPY_DN	350	-1.93	0.000	0.002
KYNG_WERNER_SYNDROM_DN	17	-1.93	0.000	0.002
MORI_LARGE_PRE_BII_LYMPHOCYTE_UP	81	-1.93	0.000	0.002
HORIUCHI_WTAP_TARGETS_DN	294	-1.92	0.000	0.002
PAL_PRMT5_TARGETS_UP	179	-1.92	0.000	0.002
VILLANUEVA_LIVER_CANCER_KRT19_UP	164	-1.92	0.000	0.002
KEGG_STEROID_BIOSYNTHESIS	17	-1.92	0.000	0.002
REACTOME_LAGGING_STRAND_SYNTHESIS	20	-1.92	0.000	0.002
REACTOME_RESOLUTION_OF_D_LOOP_STRUCTURES	31	-1.92	0.000	0.002
LI_WILMS_TUMOR_VS_FETAL_KIDNEY_1_DN	155	-1.91	0.000	0.002
REACTOME_RESOLUTION_OF_AP_SITES_VIA_THE_MULTIPLE_NUCLEOTI	25	-1.91	0.004	0.002

DE_PATCH_REPLACEMENT_PATHWAY				
WANG_RESPONSE_TO_GSK3_INHIBITOR_SB216763_DN	336	-1.90	0.000	0.002
MEISSNER_BRAIN_HCP_WITH_H3_UNMETHYLATED	25	-1.90	0.000	0.002
ZHAN_MULTIPLE_MYELOMA_CD1_VS_CD2_DN	47	-1.90	0.000	0.002
KEGG_MISMATCH_REPAIR	23	-1.90	0.000	0.002
PID_BARD1_PATHWAY	28	-1.90	0.000	0.002
TANG_SENESCENCE_TP53_TARGETS_DN	51	-1.90	0.000	0.002
REACTOME_METABOLISM_OF_STEROIDS	123	-1.90	0.000	0.002
SERVITJA_LIVER_HNF1A_TARGETS_DN	114	-1.90	0.000	0.002
VANHARANTA_UTERINE_FIBROID_UP	37	-1.90	0.000	0.002
MORI_MATURE_B_LYMPHOCYTE_DN	67	-1.89	0.000	0.002
LY_AGING_PREMATURE_DN	27	-1.89	0.002	0.002
REACTOME_RESOLUTION_OF_ABASIC_SITES_AP_SITES	38	-1.89	0.000	0.002
KRASNOSELSKAYA_ILF3_TARGETS_DN	38	-1.89	0.000	0.002
JACKSON_DNMT1_TARGETS_DN	15	-1.89	0.002	0.002
BENPORATH_PROLIFERATION	140	-1.89	0.000	0.003
REACTOME_CYTOSOLIC_SULFONATION_OF_SMALL_MOLECULES	17	-1.88	0.000	0.003
WINNEPENNINCKX_MELANOMA_METASTASIS_UP	156	-1.88	0.000	0.003
CHEN_ETV5_TARGETS_TESTIS	19	-1.88	0.000	0.003
SHAFFER_IRF4_TARGETS_IN_ACTIVATED_DENDRITIC_CELL	62	-1.88	0.000	0.003
KEGG_HEMATOPOIETIC_CELL_LINEAGE	54	-1.88	0.000	0.003
REACTOME_TELOMERE_MAINTENANCE	68	-1.88	0.000	0.003
REACTOME_CHROMOSOME_MAINTENANCE	92	-1.87	0.000	0.003
LI_INDUCED_T_TO_NATURAL_KILLER_DN	121	-1.87	0.000	0.003
REACTOME_RESOLUTION_OF_D_LOOP_STRUCTURES_THROUGH_SYNT	25	-1.86	0.002	0.004
HESIS_DEPENDENT_STRAND_ANNEALING_SDSA				
MORI_PRE_BI_LYMPHOCYTE_UP	74	-1.86	0.000	0.004
ZHANG_BREAST_CANCER_PROGENITORS_UP	396	-1.85	0.000	0.004
ODONNELL_TARGETS_OF_MYC_AND_TFRC_DN	43	-1.85	0.000	0.004
KIM_MYCN_AMPLIFICATION_TARGETS_UP	82	-1.84	0.000	0.005
LINDGREN_BLADDER_CANCER_CLUSTER_3_UP	306	-1.84	0.000	0.005
PETROVA_ENDOTHELIUM_LYMPHATIC_VS_BLOOD_UP	112	-1.83	0.000	0.006
REACTOME_MISMATCH_REPAIR	15	-1.83	0.000	0.006
KEGG_BASE_EXCISION_REPAIR	33	-1.83	0.000	0.006
PODAR_RESPONSE_TO_ADAPHOSTIN_DN	16	-1.83	0.002	0.006
WANG_CISPLATIN_RESPONSE_AND_XPC_UP	154	-1.83	0.000	0.006
KAUFFMANN_DNA_REPAIR_GENES	225	-1.82	0.000	0.007
VERHAAK_AML_WITH_NPM1_MUTATED_DN	200	-1.82	0.000	0.007
WONG_EMBRYONIC_STEM_CELL_CORE	325	-1.81	0.000	0.008
BOYLAN_MULTIPLE_MYELOMA_C_UP	43	-1.80	0.000	0.008
TOYOTA_TARGETS_OF_MIR34B_AND_MIR34C	417	-1.80	0.000	0.009
ZHENG_GLIOBLASTOMA_PLASTICITY_UP	209	-1.80	0.000	0.009

SCHAEFFER_SOX9_TARGETS_IN_PROSTATE_DEVELOPMENT_DN	40	-1.80	0.000	0.009
SLEBOS_HEAD_AND_NECK_CANCER_WITH_HPV_UP	72	-1.79	0.000	0.009
VECCHI_GASTRIC_CANCER_EARLY_UP	388	-1.79	0.000	0.010

Supplementary Table S7.

Enriched pathways and processes characteristic of upregulated genes in both PTC596 single and bortezomib single in our RNA-seq (FDR p <0.05, top 50).

term_id	term_name	p_value	negative_log10_of _p_value
GO:0003735	structural constituent of ribosome	0.000	280.9
GO:0044391	ribosomal subunit	0.000	276.0
KEGG:03010	Ribosome	0.000	269.5
GO:0005840	ribosome	0.000	256.2
REAC:R-HSA-72766	Translation	0.000	203.7
GO:0005198	structural molecule activity	0.000	177.3
GO:0006412	translation	0.000	176.0
GO:0043043	peptide biosynthetic process	0.000	174.1
GO:0022626	cytosolic ribosome	0.000	174.0
GO:1990904	ribonucleoprotein complex	0.000	172.5
WP:WP477	Cytoplasmic Ribosomal Proteins	0.000	167.0
GO:0006518	peptide metabolic process	0.000	163.9
GO:0043604	amide biosynthetic process	0.000	163.9
REAC:R-HSA-156902	Peptide chain elongation	0.000	157.0
REAC:R-HSA-192823	Viral mRNA Translation	0.000	157.0
GO:0006614	SRP-dependent cotranslational protein targeting to membrane	0.000	155.0
GO:0015934	large ribosomal subunit	0.000	154.3
REAC:R-HSA-2408557	Selenocysteine synthesis	0.000	153.4
REAC:R-HSA-156842	Eukaryotic Translation Elongation	0.000	153.4
REAC:R-HSA-72764	Eukaryotic Translation Termination	0.000	153.4
REAC:R-HSA-975956	Nonsense Mediated Decay (NMD) independent of the Exon Junction Complex (EJC)	0.000	151.7
GO:0006613	cotranslational protein targeting to membrane	0.000	151.7
GO:0043603	cellular amide metabolic process	0.000	148.5
REAC:R-HSA-72689	Formation of a pool of free 40S subunits	0.000	147.3
GO:0045047	**protein targeting to ER**	**0.000**	**147.1**
GO:0072599	**establishment of protein localization to endoplasmic reticulum**	**0.000**	**145.1**
REAC:R-HSA-156827	L13a-mediated translational silencing of Ceruloplasmin expression	0.000	141.3
GO:0000184	nuclear-transcribed mRNA catabolic process, nonsense-mediated decay	0.000	141.0
REAC:R-HSA-72706	GTP hydrolysis and joining of the 60S ribosomal subunit	0.000	140.7
REAC:R-HSA-1799339	SRP-dependent cotranslational protein targeting to membrane	0.000	140.7
REAC:R-HSA-975957	Nonsense Mediated Decay (NMD) enhanced by the Exon Junction Complex (EJC)	0.000	139.1
REAC:R-HSA-927802	Nonsense-Mediated Decay (NMD)	0.000	139.1

REAC:R-HSA-2408522	Selenoamino acid metabolism	0.000	138.6
REAC:R-HSA-72737	Cap-dependent Translation Initiation	0.000	137.1
REAC:R-HSA-72613	Eukaryotic Translation Initiation	0.000	137.1
GO:0070972	protein localization to endoplasmic reticulum	0.000	135.1
GO:0044445	cytosolic part	0.000	131.9
REAC:R-HSA-168273	Influenza Viral RNA Transcription and Replication	0.000	131.4
REAC:R-HSA-168255	Influenza Life Cycle	0.000	128.0
REAC:R-HSA-168254	Influenza Infection	0.000	124.2
GO:0019083	viral transcription	0.000	123.4
GO:1901566	organonitrogen compound biosynthetic process	0.000	120.5
GO:0019080	viral gene expression	0.000	120.1
CORUM:306	Ribosome, cytoplasmic	0.000	119.9
GO:0006612	protein targeting to membrane	0.000	119.5
GO:0006413	translational initiation	0.000	118.8
REAC:R-HSA-9010553	Regulation of expression of SLITs and ROBOs	0.000	118.8
GO:0000956	nuclear-transcribed mRNA catabolic process	0.000	116.2
REAC:R-HSA-6791226	Major pathway of rRNA processing in the nucleolus and cytosol	0.000	115.7

Supplementary Table S8.

List of primers used for Quantitative RT-PCR.

Sequences of primers used for quantitative real time PCR.

Target Gene	Primers	Sequences (5' to 3')
BMI1	Forward	CGTGTATTGTTCGTTACCTGGA
	Reverse	TTCAGTAGTGGTCTGGTCTTGT
mBmi1	Forward	AAACCAGACCACTCCTGAACA
	Reverse	TCTTCTTCTCTTCATCTCATTTTTGA
DDIT3	Forward	AGAACCAGGAAACGGAAACAGA
	Reverse	TCTCCTTCATGCGCTGCTTT
HSPA5	Forward	CAATCAAGGTCTATGAAGGTGAAAGA
	Reverse	CACATCTATCTCAAAGGTGACTTCAATC
ATF4	Forward	CCCTTCACCTTCTTACAACCTC
	Reverse	TGCCCAGCTCTAAACTAAAGGA
GAPDH	Forward	CTGACTTCAACAGCGACACC
	Reverse	TAGCCAAATTCGTTGTCATACC
ACTB	Forward	GGATGCAGAAGGAGATCACTG
	Reverse	CGATCCACACGGAGTACTTG

Supplementary Figure S1.

A

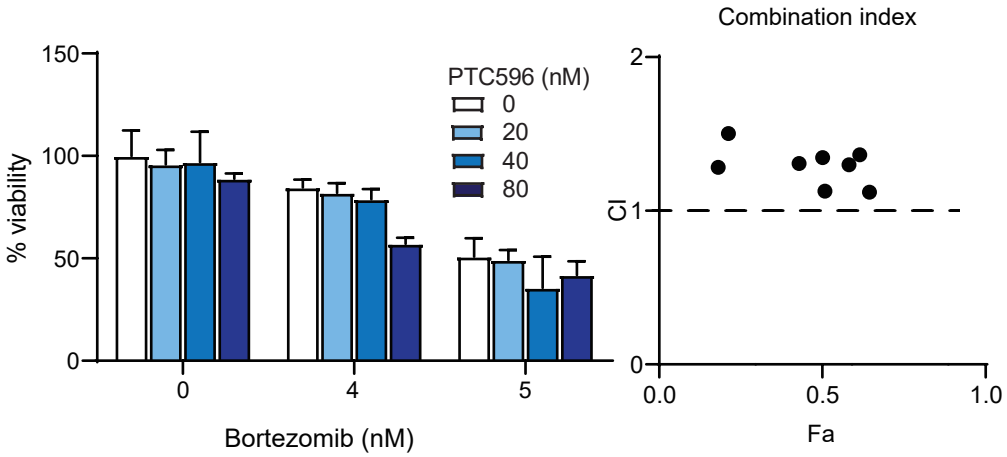

Supplementary Figure S1. PTC596 and bortezomib do not exert synergistic anti-MM activity without BMSCs. (A) MTS assay of MM.1S cells treated with the indicated doses of PTC596 for 48 hours and bortezomib for the last 24 hours. The y-axis presents percent viability relative to the untreated control. Data are shown as means ± SD of triplicate samples. Combination index values are shown in the right graph.

Supplementary Figure S2.

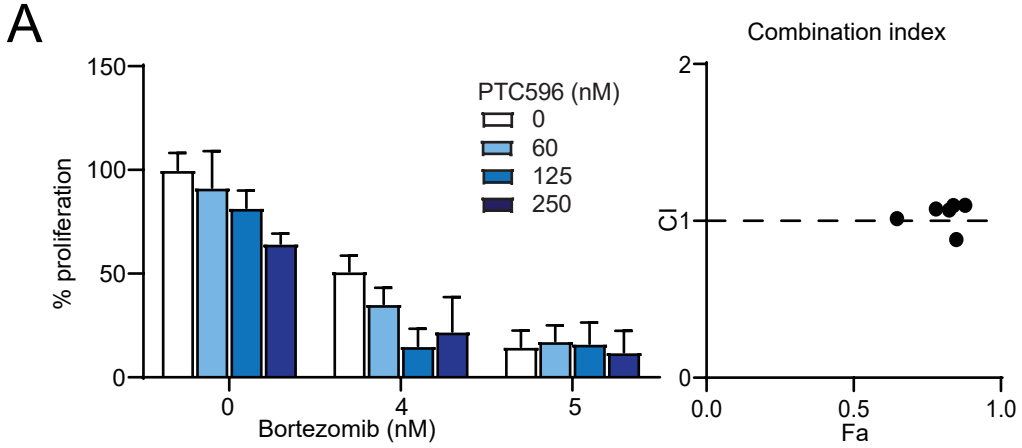

Supplementary Figure S2. PTC596 and bortezomib exert additive anti-MM activity when the cells are co-cultured with BMSCs

(A) BrdU proliferation assay of OPM-2 cells co-cultured with BMSCs derived from MM patients upon treatment with the indicated doses of PTC596 and bortezomib for 48 hours. Results of triplicate experiments and combination index values are shown in the left and right graphs, respectively.

Supplementary Figure S3.

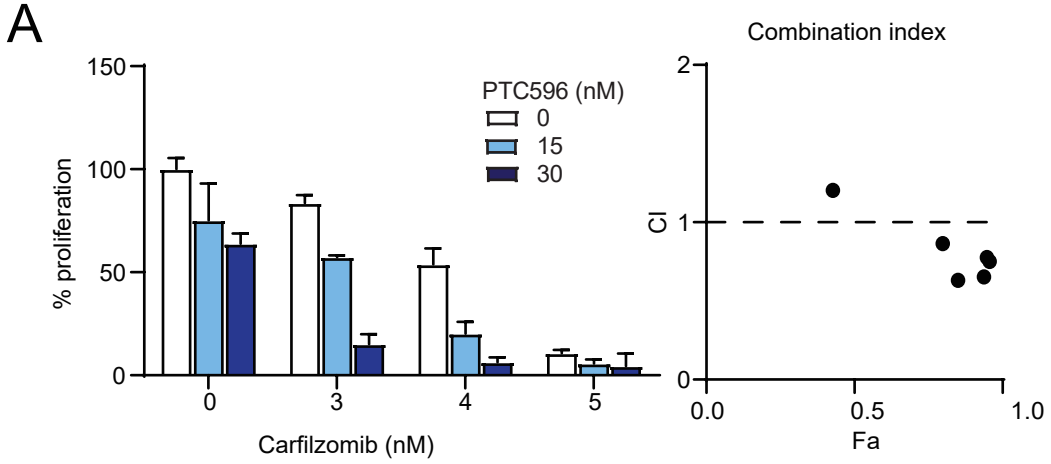

Supplementary Figure S3. PTC596 and carfilzomib exert synergistic anti-MM activity when the cells are co-cultured with BMSCs

(A) BrdU proliferation assay of MM.1S cells co-cultured with BMSCs derived from MM patients upon treatment with the indicated doses of PTC596 and carfilzomib for 48 hours. Results of triplicate experiments and combination index values are shown in the left and right graphs, respectively.

Supplementary Figure S4.

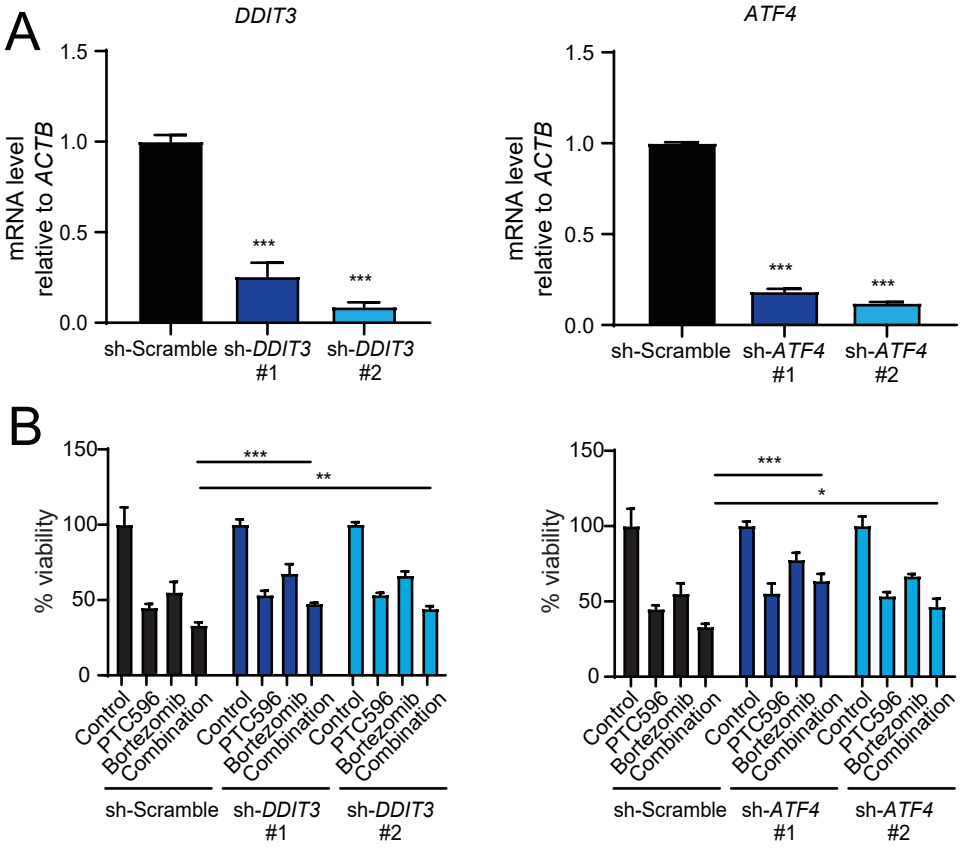

Supplementary Figure S4. ER stress pathway contributes to the cytotoxicity of the combination treatment.
(A, B) RPMI8226 cells transduced with the indicated lentiviruses were selected by puromycin. Those were subjected to quantitative RT-PCR (A) and MTS assays (B). (A) Quantitative mRNA expression of *DDIT3* and *ATF4*. Y-axis represents fold change after normalization to *ACTB* and error bars represent SD of triplicates. ***P < 0.001 by one-way ANOVA. (B) MTS assays of RPMI8226 cells transduced with sh-*DDIT3* and sh-Scramble lentiviruses (left graphs), and RPMI8226 cells transduced with sh-*ATF4* and sh-Scramble lentiviruses (right graphs), treated with or without PTC596 (15 nM) in the presence or absence of bortezomib (6 nM) for 48 hours. The y-axis presents percent viability relative to the untreated control. Data are shown as means ± SD of triplicate samples. *P < 0.05; **P < 0.01; *** P < 0.001 using Student' s *t*-test.

Supplementary Figure S5.

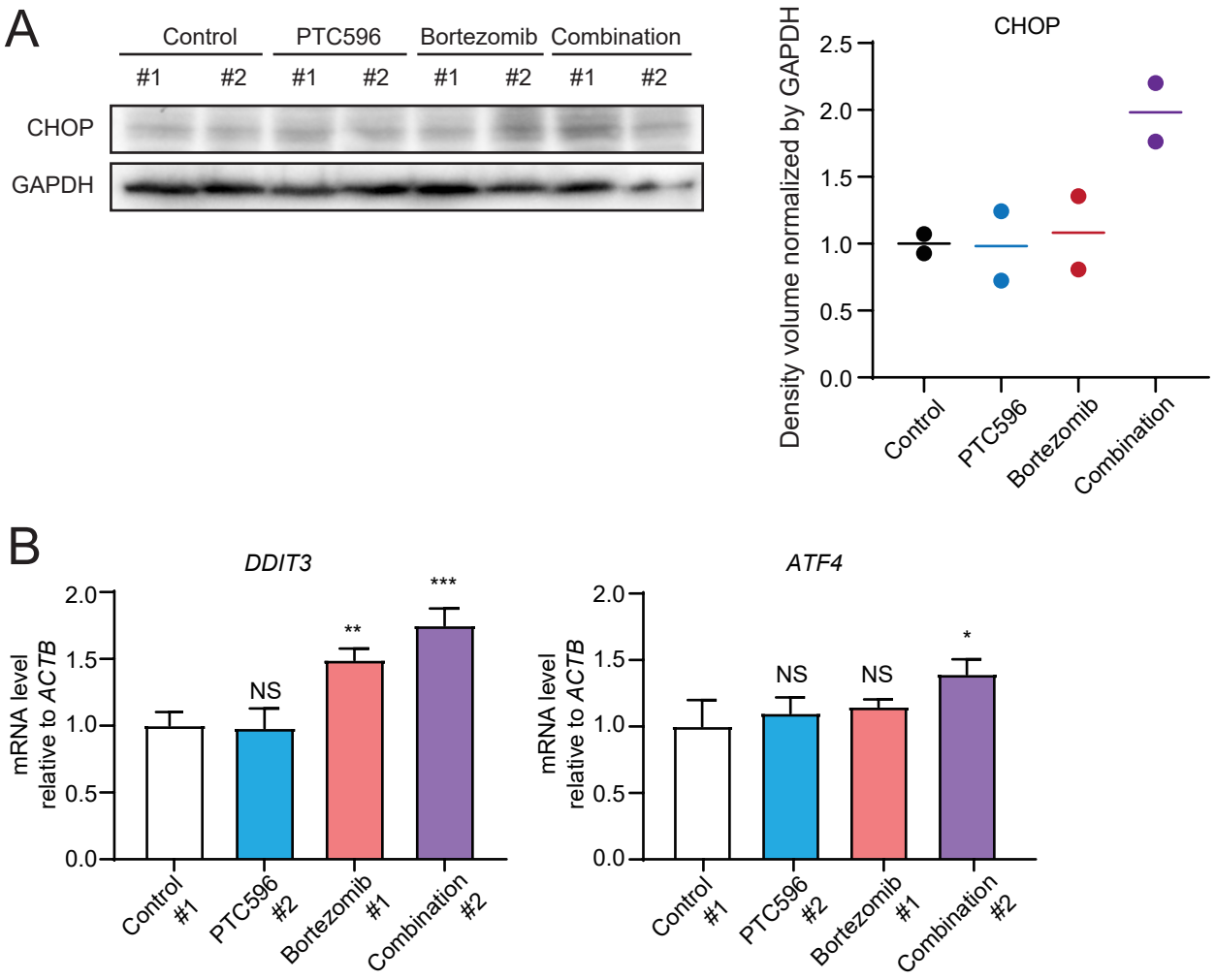

Supplementary Figure S5. Endoplasmic reticulum stress is augmented by the combination of PTC596 and bortezomib *in vivo*.

(A, B) Tumors harvested from mice treated for 2 weeks with oral PTC596 (6.25 mg/kg) twice a week, subcutaneous bortezomib (0.5 mg/kg) twice a week, or the combination were subjected to western blotting (A) and RT-PCR (B). (A) Western blotting analysis of the indicated proteins in MM tumor cells. GAPDH served as a loading control. The right graphs show the density volume normalized by GAPDH. (B) Quantitative RT-PCR of mRNA expression of *DDIT3* and *ATF4*. *ACTB* was used to normalize the amount of input RNA. Data are shown as mean ± SD (n=3). *P < 0.05; **P < 0.01; *** P < 0.001; ns, not significant using one-way ANOVA.Y-axis represents fold change after normalization to *ACTB*, and error bars represent SD of triplicates.

Supplementary Figure S6.

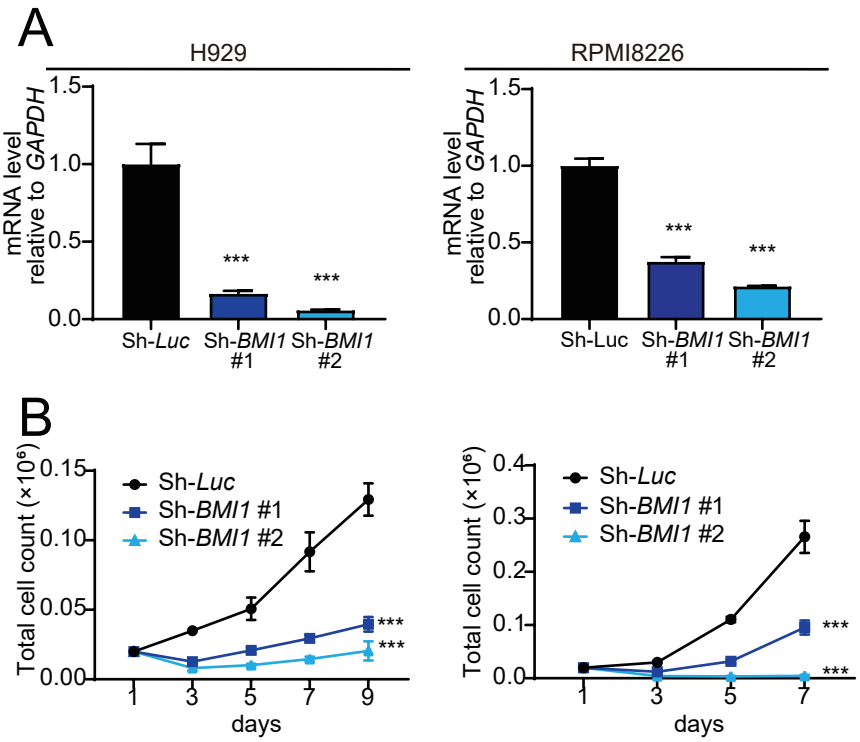

Supplementary Figure S6. MM cells depend on BMI1 for their growth.

(A, B) Human MM cell lines H929 and RPMI8226 cells transduced with the indicated lentiviruses were selected by cell sorting for GFP expression. Those were subjected to quantitative RT-PCR (A) and cell counting assay (B). (A) Quantitative RT-PCR of mRNA expression of *BMI1*. Y-axis represents fold change after normalization to *GAPDH*, and error bars represent SD of triplicates. ***P < 0.001 by one-way ANOVA. (B) Cell counting assay using trypan blue on the indicated days of cultures. Data represent mean ± SD of triplicate cultures. ***P < 0.001 by one-way ANOVA.

Whole blots for cropped images

Whole blot for cropped image for figure 2A

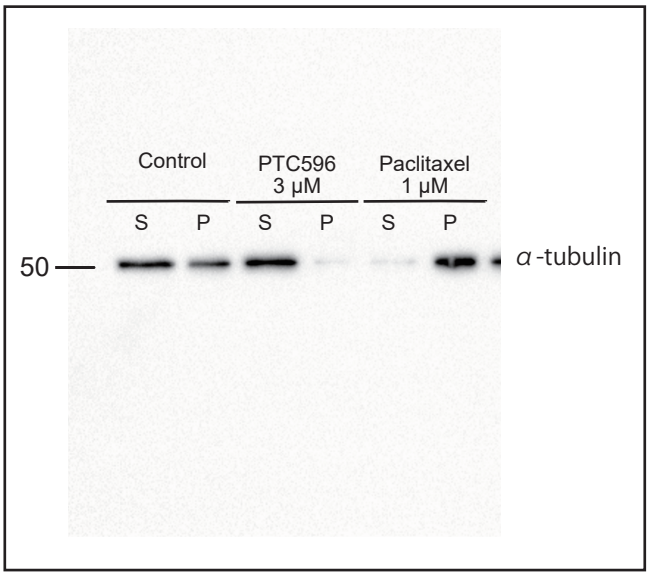

Whole blots for cropped images for figure 3C

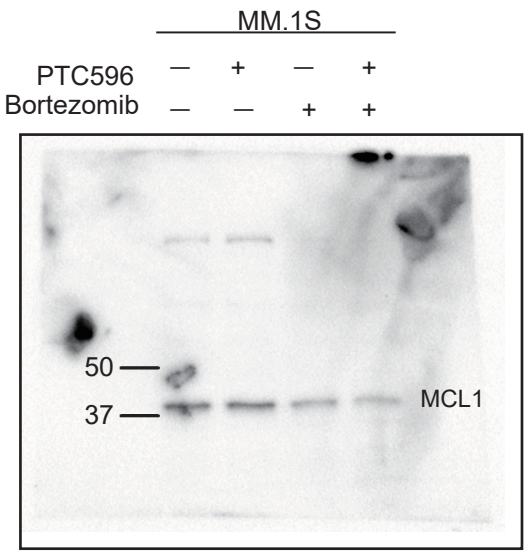

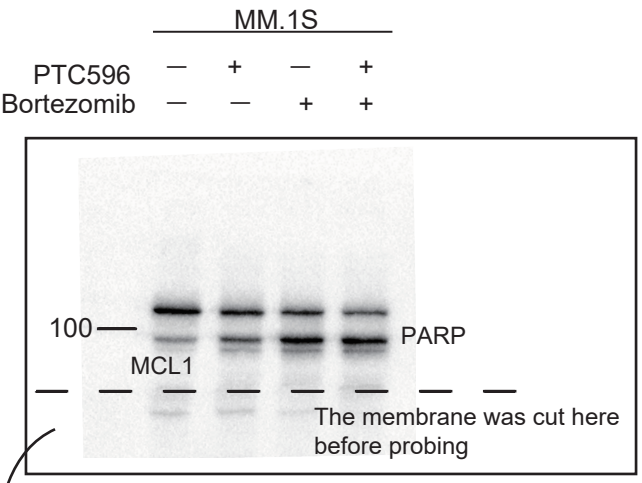

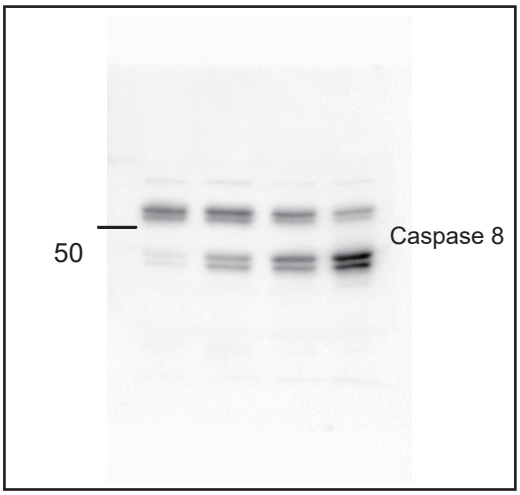

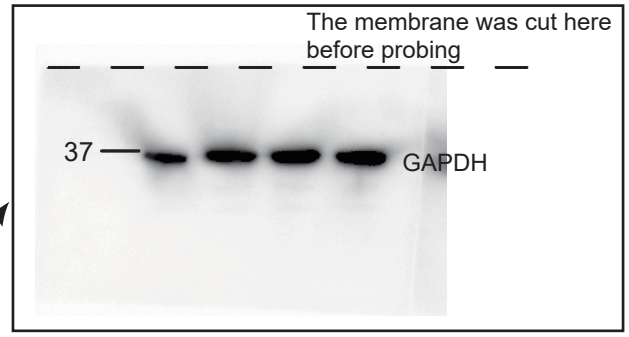

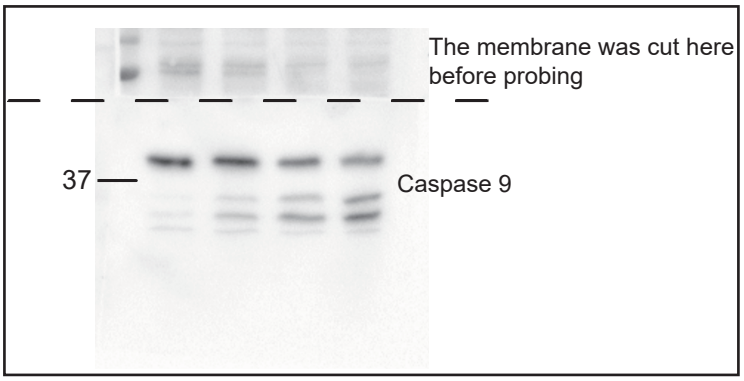

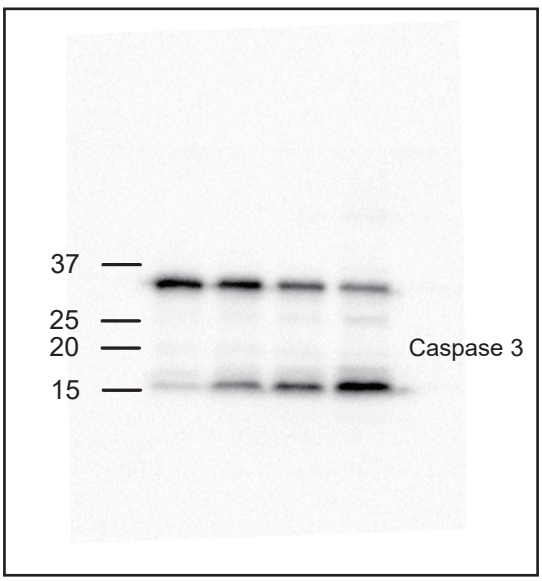

Whole blots for cropped images for figure 3C

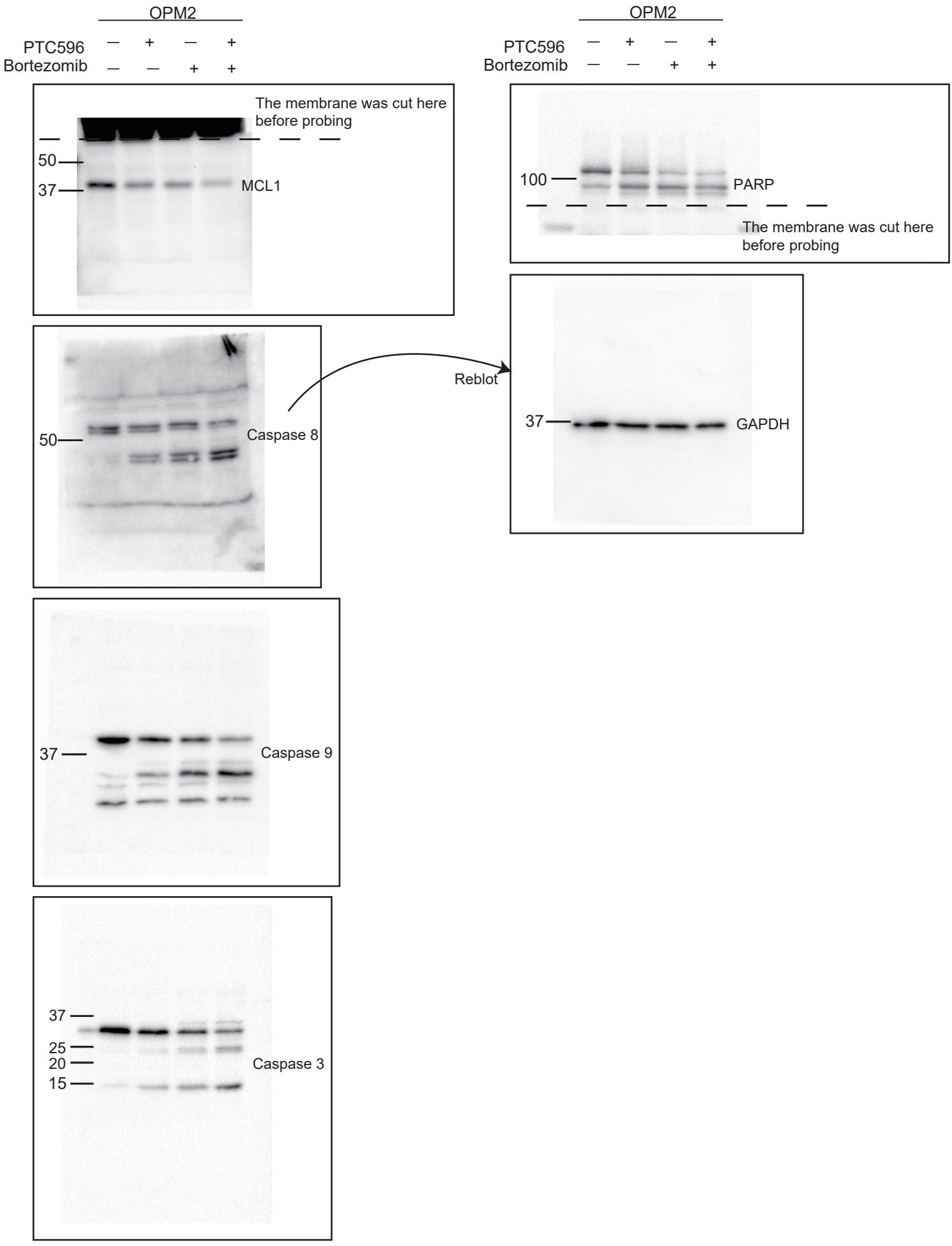

Whole blots for cropped images for figure 5B

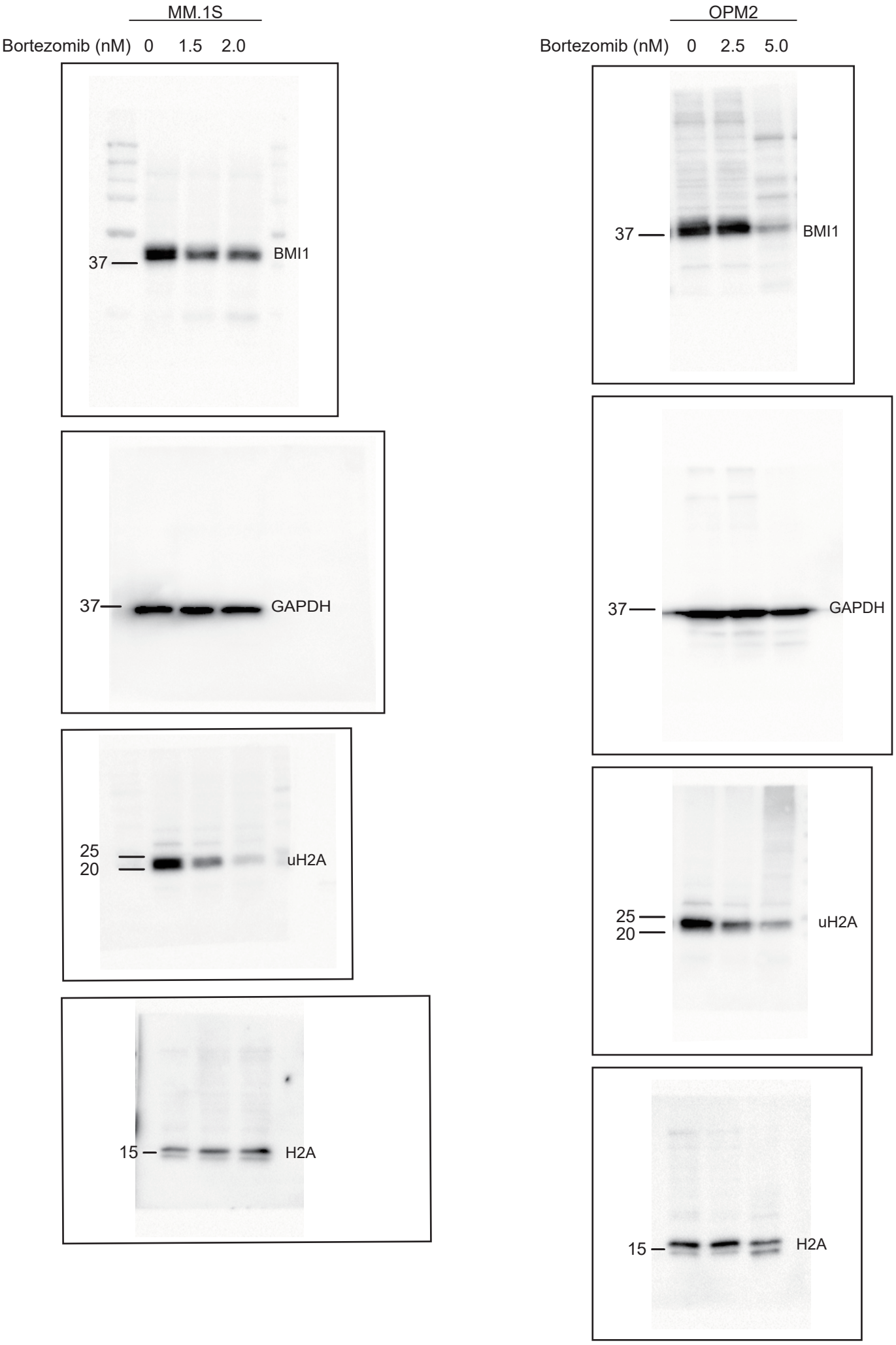

Whole blots for cropped images for figure 5C

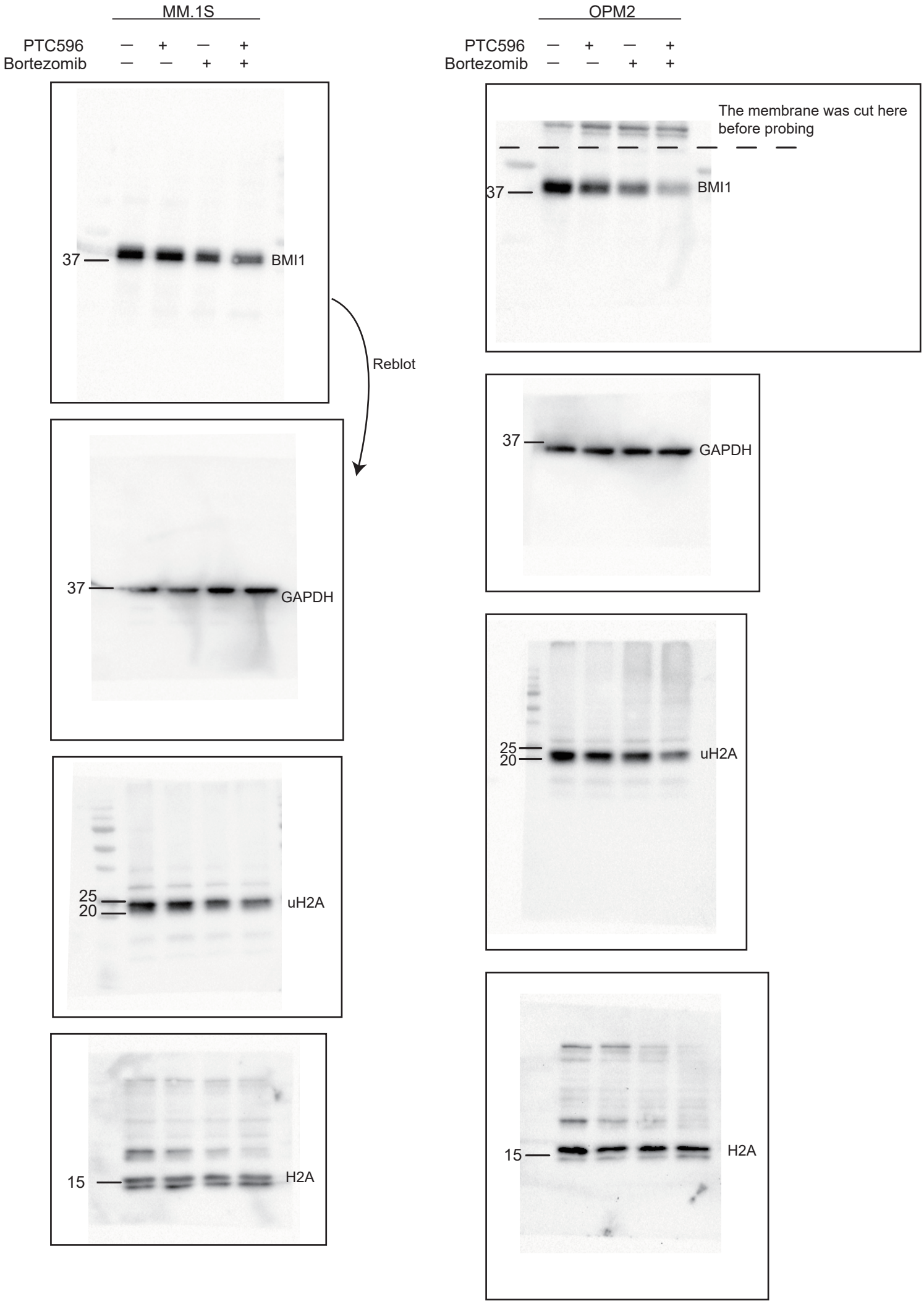

Whole blots for cropped images for figure 6C

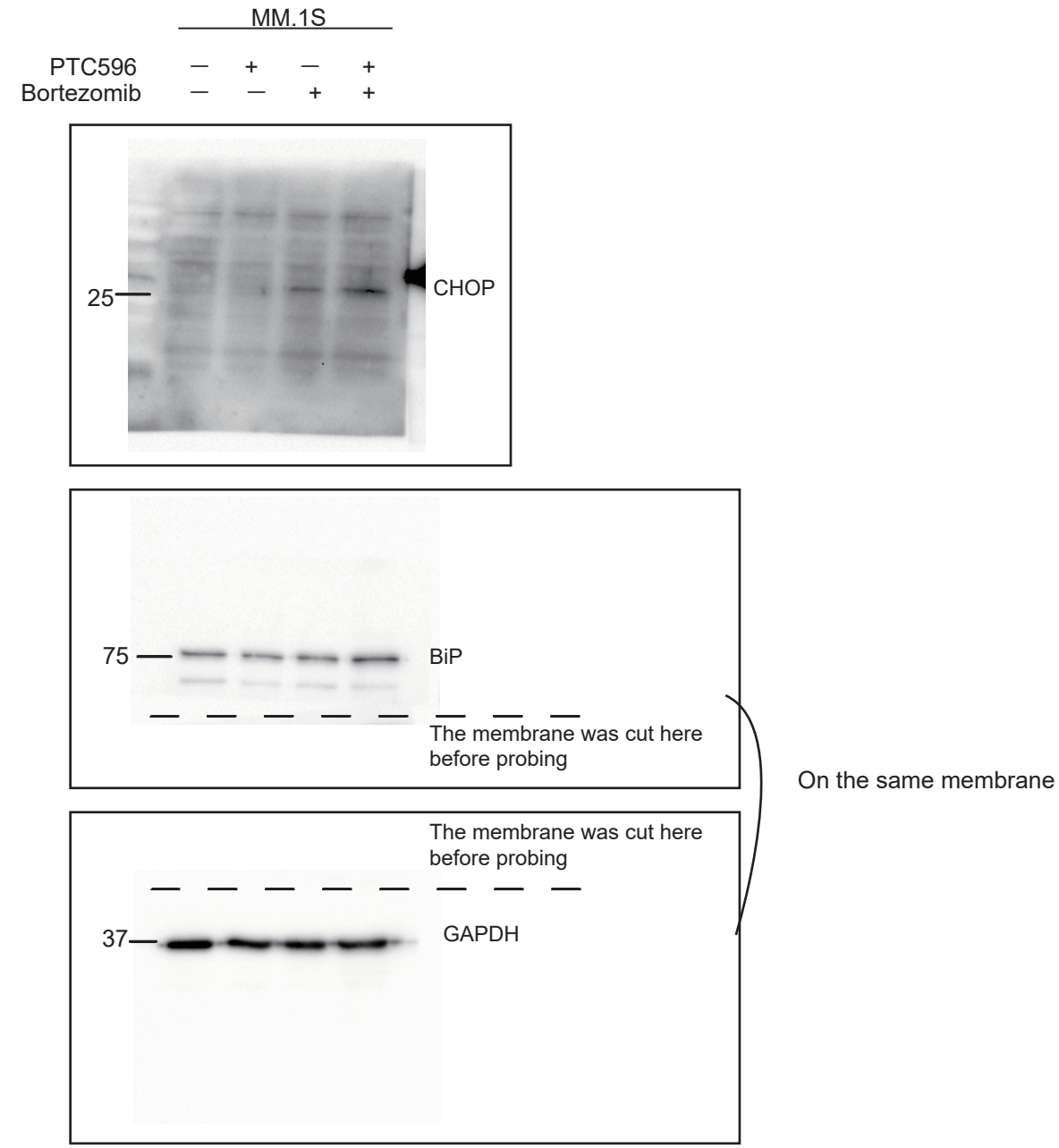

Whole blots for cropped images for supplementaly figure 5A

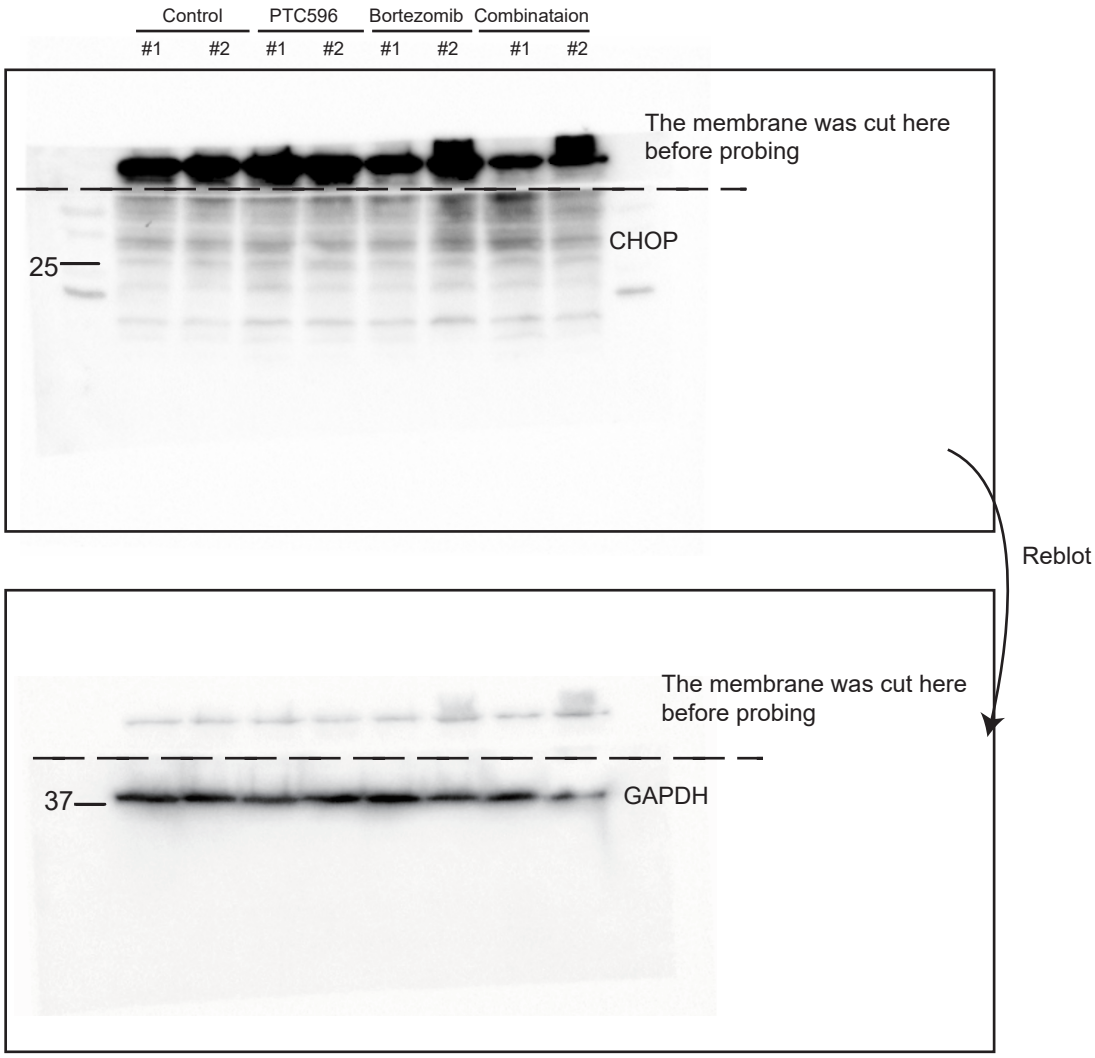

Scientific Reports 11, Article number: 2074 (2021)

2021 年 1 月 22 日　公表済

DOI: 10.1038/s41598-021-81577-x